TAMPEREEN TEKNILLINEN YLIOPISTO
TAMPERE UNIVERSITY OF TECHNOLOGY

TERO ILVESMÄKI

NEURAL TRACT ANALYSIS; A SOFTWARE IMPLEMENTATION

Master of Science Thesis

Examiners: Prof. Ilpo Vattulainen and Prof. Hannu Eskola
Examiners and topic approved in the Science and Environmental Engineering Faculty Council meeting on 3rd of October 2012

ABSTRACT

TAMPERE UNIVERSITY OF TECHNOLOGY
Master's Degree Programme in Science and Technology
TERO ILVESMÄKI : Neural tract analysis; a software implementation
Master of Science Thesis, 63 pages, 11 Appendix pages
November 2012
Major: Advanced Engineering Physics
Examiners: Prof. Ilpo Vattulainen and Prof. Hannu Eskola
Keywords: MRI, DTI, voxelwise analysis, neural tract, FSL, TBSS

Diffusion magnetic resonance imaging (MRI) is an imaging modality that can be used to examine the microstructure of white matter in the human brain, which cannot be seen by other means of imaging. This microstructure can be derived from diffusion based fractional anisotropy (FA) images, which can be correlated to the neural tract structures. Fractional anisotropy is basically a scalar value representing the isotropy of water molecule diffusion in a medium. Various neurological conditions affect neural tract and axonal structures, and these changes in neural tracts can be visualized via diffusion MRI and FA value comparisons.

FMRIB Software Library (FSL) is a collection of tools for magnetic resonance imaging data processing and analyses. In this thesis, a diffusion group comparison tool, Tract-Based Spatial Statistics (TBSS), is used to determine differences between two groups of diffusion images. The other group consists of spinal injury patients and the other of healthy volunteers. TBSS creates a skeleton model of neural tract structure, projecting the maximum FA values to the skeleton, and compares these skeletons by a two-sample statistical t-test. The program reports any areas with statistical differences according to their corresponding p-value.

FA values of these two groups were tested for statistically significant differences, and large areas of lowered FA values were found in the patient group when compared to the control group. However, these large areas of lowered FA are present not because of the structural changes in neural tracts caused by the spinal injury, but because of age related effects on tract integrity. The implementation itself is a success even though the results are biased in a sense; areas of lowered FA are found in locations where such effect is expected to be seen from the effects of age. Thus the method can be deemed functional, but new analyses are required for correct results on effects of the injury on white matter structure.

TIIVISTELMÄ

TAMPEREEN TEKNILLINEN YLIOPISTO
Teknis-luonnontieteellinen koulutusohjelma
TERO ILVESMÄKI: Hermorata-analyysi; ohjelmistosovellutus
Diplomityö, 63 sivua, 11 liitesivua
Marraskuu 2012
Pääaine: Teknillinen fysiikka
Tarkastajat: Prof. Ilpo Vattulainen ja Prof. Hannu Eskola
Avainsanat: MRI, DTI, vokselipohjainen analyysi, hermorata, FSL, TBSS

Diffuusiomagneettikuvaus on suosittu ja monipuolinen kuvausmodaliteetti. Diffuusiokuvauksen avulla voidaan selvittää mikroskooppisia rakenteita aivoista, sekä muualta hermokudoksesta, joita ei muilla tavoin voida havaita. Nämä rakenteet saadaan näkyviin johtamalla diffuusiodatasta fraktionaaliseen anisotropiaan (FA) pohjautuvia kuvia. FA-arvo sekä -kartat voidaan rinnastaa aivojen valkean aineen hermoratarakenteeseen, jossa FA-arvo kuvastaa vesimolekyylin diffuusion isotrooppisuutta tietyssä kuvaelementissä. Hermoratojen rakenteeseen vaikuttavat useat neurologiset sairaudet, joiden vaikutusta voidaan tutkia FA-arvojen avulla, vertaamalla terveiden vapaaehtoisten ryhmän FA arvoja potilasryhmän vastaaviin.

Oxfordin yliopiston kehittämä ohjelmisto, FMRIB Software Library (FSL), on kokoelma magneettikuvien käsittelyyn ja analyysiin luotuja työkaluja. Tässä diplomityössä keskitytään käyttämään ohjelmistoon kuuluvaa diffuusiokuvien ryhmävertailutyökalua: Tract-Based Spatial Statistics (TBSS). Työkalulla voidaan vertailla ryhmien välisiä tilastollisesti merkittäviä eroja FA arvoissa. Ohjelma luo jokaisen kohteen FA kartoista luurankomallit, jotka vastaavat hermoratakimppujen sijaintia sekä niissä olevaa maksimi FA arvoa. Näitä luurankomalleja vertaillaan kahden otoksen t-testin avulla, ja tuloksena ohjelma raportoi alueet joissa ryhmien välillä on tilastollisesti merkittäviä eroja FA arvoissa sekä niiden merkittävyyden p-arvon avulla. Diplomityön analyysissa käytettiin selkärankavammapotilaiden ryhmää, jota vertailtiin terveistä vapaaehtoisista koostuneeseen verrokkiryhmään.

Käytettyjen ryhmien väliset FA arvot poikkesivat merkittävästi toisistaan; selkärankavammapotilailla oli laajoja alueita, joissa FA arvot olivat alempia verrokkiryhmään nähden. Tulokset olivat kuitenkin virheelliset, sillä laajat eroavat alueet johtuivat ennemmin iän vaikutuksesta hermoratojen rakenteeseen, kuin itse vammasta. Koska ryhmien ikäjakaumat erosivat toisistaan huomattavasti; potilasryhmän keskiikä oli huomattavasti verrokkiryhmää korkeampi, dominoi iän vaikutus siis saatuja tuloksia. Metodin soveltaminen neurologisiin tarkoituksiin oli kuitenkin onnistunut, sillä tuloksissa näkynyt iän vaikutus esiintyi alueilla joissa tapahtuu odotettavasti hermoratojen rappeutumista iän myötä. Oikeiden tulosten tuottamiseksi analyysi tulee kuitenkin ajaa uudelleen paremmin ikävastaavilla ryhmillä.

PREFACE

This Master of Science Thesis was done in cooperation with the Department of Biomedical Engineering and the Department of Physics between June and November 2012. Implementation of the software addressed in this thesis was done at Tampere University Hospital with equipment provided by Pirkanmaa Hospital District. I would like to acknowledge the hospital for providing the necessary tools and funding for the thesis.

I would like to thank my examiners, professor Hannu Eskola and professor Ilpo Vattulainen, for their support, guidance and feedback on the thesis. I would like to thank Hannu Eskola also for the opportunity to work on such an interesting project.

I am grateful to Pertti Ryymin and Ullamari Hakulinen for all the help and guidance they have provided throughout the whole process of my M.Sc thesis.

In addition I would like to give special thanks to everyone who supported me during the writing process; my girlfriend, family and closest friends.

Tampere, November 27, 2012.

Tero Ilvesmäki

CONTENTS

ABBREVIATIONS

MRI	magnetic resonance imaging
FA	fractional anisotropy
FSL	FMRIB Software Library
TBSS	Tract-Based Spatial Statistics
RF	radio frequency
MR	magnetic resonance
NMR	nuclear magnetic resonance
SE	spin echo
PGSE	pulsed gradient spin echo
ADC	apparent diffusion coefficient
DTI	diffusion tensor imaging
MS	multiple sclerosis
TBI	traumatic brain injury
ROI	region of interest
FMRIB	Functional MRI of the Brain
NiFTI	Neuroimaging Informatics Technology Initiative
GUI	graphical user interface
FAQ	frequently asked questions
DICOM	Digital Imaging and Communications in Medicine
BET	Brain Extraction Tool
GLM	general linear model
DoF	degrees of freedom
MNI	Montreal Neurological Institute
FWHM	full width at half maximum
TFCE	Threshold-Free Cluster Enhancement
FWE	familywise error

1. INTRODUCTION

Magnetic resonance imaging is one of the most popular imaging modalities applied for neurological purposes at present. It is also the imaging modality with the most interesting future prospects. For example diffusion MRI is constantly used for brain connectivity analyses. Analysis of nervous system structural changes and lesions is important in recognizing different type of structural neurological disorders and their possible impact on neural tract structures. A significant amount of research is being done in order to discover novel ways of efficiently analyzing neurological image data for possible lesions and abnormalities connected to various types of neurological disorders. Diffusion magnetic resonance images need to be processed in order to extract the desired analytical information of neurologically important structures; in this thesis a method for processing raw diffusion images and using the images in a statistical multi-subject analysis is reviewed in detail.

FMRIB Software Library is a software compilation made for the analysis of MRI data. [1] [2] The software comprises a broad selection of MRI data analysis tools for structural, functional and diffusion MRI data. Most of the diffusion MRI tools will be reviewed, but emphasis will be on group analysis of fractional anisotropy maps by utilizing a tool for neural tract based analysis (Tract-Based Spatial Statistics, TBSS [3]). Diffusion image data of spinal injury patient group and a healthy control group will be analyzed and compared via brain white matter fractional anisotropy values. The analysis process and software will be evaluated and its usefulness reviewed in terms of efficiency and performance.

Research based on FSL has been done frequently in the past few years, and the method has been remarkably popular among neurological researchers. Although the software and its underlying mechanics have downfalls, it still has its place in the field of neurology. This thesis is a part of an attempt to utilize FSL software in clinical research in neurological disorders either as a direct method or as a supporting tool.

2. MAGNETIC RESONANCE IMAGING

Magnetic resonance imaging is an imaging modality that is most often used for high resolution soft tissue imaging via spin relaxation times. Strong magnetic fields and radio frequency (RF) electromagnetic waves are used in combination to create magnetic resonance (MR) images. The main functional parts of MR scanners consist of the following:

- large main coil that creates a homogeneous magnetic field around the patient,
- three smaller coils for producing spatial encoding magnetic gradients (measured in mT/m)
- and a RF transceiver that emits and receives RF signals.

Usually the magnetic field strength in MRI is about 1,5 – 3T in diagnostic applications but fields of 7T and up can be used in research purposes. The scanner also includes a central processing unit used for coordination of the scan process and data processing. Because this research is based on diffusion imaging mode rather than any of the basic T1 or T2 -weighted (spin-spin and spin-lattice relaxation times respectively) MRI, they will not be explained in this text. The main focus will instead be on the imaging mode of MRI which visualizes molecular diffusion processes in the imaged medium.

2.1 Nuclear magnetic resonance

Magnetic resonance imaging is based on a phenomenon called nuclear magnetic resonance (NMR). NMR can be observed when a nucleus with nonzero nuclear magnetic quantum number is placed in a constant magnetic field. The nucleus and its state is then disrupted by a photon, which causes the nucleus to make a transition to a higher state by resonance absorption. The amount of energy absorbed and thus also emitted (resonance) by the nucleus depends on the type of nucleus and the strength of the magnetic field surrounding it. In addition, the surrounding chemical environment also has a slight effect on the resonance frequency of the emitted photon. If a nucleus has an even amount of protons and neutrons their spins cancel each other out, the nucleus' overall spin is zero and the nucleus is not affected by NMR. [4, pp. 483–486] [5]

The principle of NMR is easiest to apprehend by considering a simple case of hydrogen atom, for which the nucleus is a single proton. The proton has two possible energy states in the presence of an external magnetic field: higher energy state where the magnetic moment of the proton is antiparallel to the external field, and lower energy state where the internal magnetic moment is parallel to the external field. If a bunch of hydrogen atoms are irradiated with radio wave photons (photons in MHz frequency range), some of the nuclei make transitions to the higher energy state and afterwards decay to the lower energy state by emitting a photon of the same energy as they absorbed. Because of the frequency of the emitted photons, the emitted radiation is called RF radiation, and by measuring this frequency one can determine the magnetic moment of the proton. [6, pp.590–591]

When a hydrogen atom is a part of a molecule, the magnetic field in its nucleus is affected by the external field and the magnetic field caused by its surrounding elements. The resonance frequency that is measured is proportional to the total magnetic field seen by the proton, and can give information on the internal magnetic field seen in the molecule. [6, pp.590–591]

In quantum mechanical terms the proton's spin precesses about the external magnetic field vector, and by disturbing this mechanism with certain RF radiation the nucleus can be induced to shift to a higher energy state. Absorption of energy in this transition to a higher energy state and relaxation of the induced state is the basis of NMR methods. [5]

2.2 Diffusion weighted imaging

In a static magnetic field a proton's spin precesses around the direction of magnetic flux density. A certain sequence involving proton spins, magnetic gradients and RF signals is used to obtain MR images; this particular sequence is called spin echo (SE) sequence. In a spin echo sequence used in conventional MRI, a 90° defocussing RF pulse is applied, which forces the spin rotation of protons in to the X-Y -plane. The transverse magnetization begins to de-phase, and a 180° defocussing RF pulse is introduced at some time point after the 90° pulse, which rotates the spin 180° around the X-axis. In theory this causes the spins to eventually re-phase and produce a signal called spin echo. The spin echo pulse sequence can be seen in figure 2.1. The strength of the echo signal varies according to the position of the proton via the inhomogeneous magnetic field. [7] [8, pp. 87–88] [9, pp. S210–S212]

In temperatures above 0 K every particle is in a constant movement known as the Brownian motion, caused by thermal energy. This diffusion motion can be visualized with a slightly different spin echo sequence, called pulsed gradient spin echo (PGSE) sequence. The method is otherwise similar to the conventional SE sequence, but two additional magnetic field gradient pulses are introduced. The two gradient pulses are

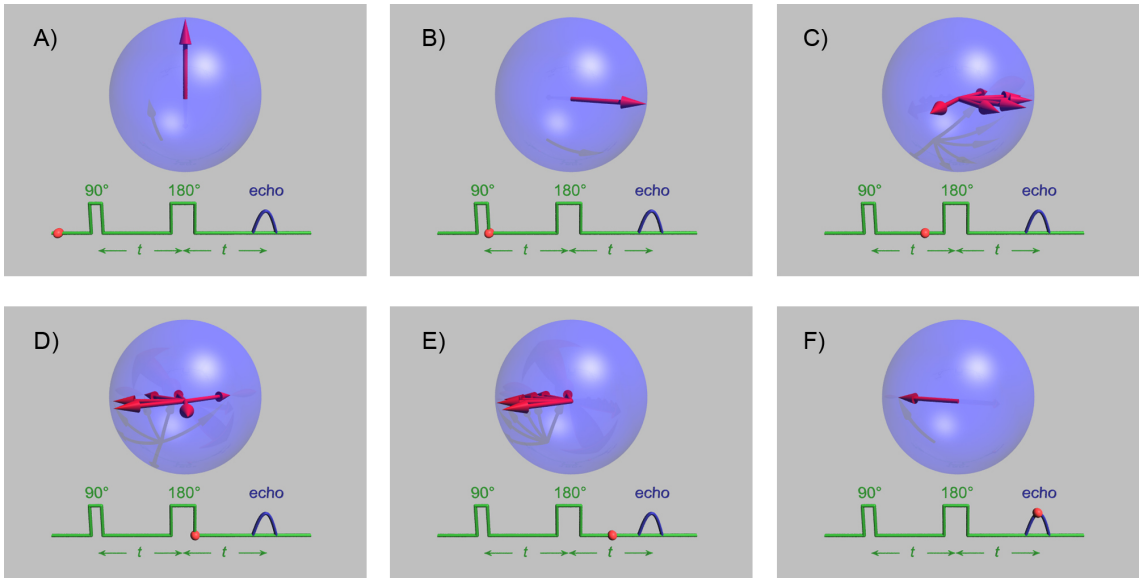

Figure 2.1: Spin echo pulse sequence. A) The red arrow represents the average spin vector of a group of protons. B) A 90° RF pulse is administered and the average spin is rotated to the X–Y -plane. C) Local magnetic field inhomogeneities cause some of the spins to speed up and some to slow down, causing signal decay. D) Applying the re-phasing 180° RF pulse reverses the situation; the slower spins are now ahead and faster spins are trailing behind. E) The faster spins are catching up with the slower spins ahead. F) The spins have completely refocused and an echo signal can be measured. [10]

positioned symmetrically about the 180° pulse, and their purpose is to create phase shifts in spins of protons that have diffused in respect to their original location. The first gradient pulse creates a phase shift depending on the strength of the gradient field at the current position of the proton. After the first gradient pulse, the 180° RF pulse is applied to re-phase the spins. A proton that has remained in its original position experience no phase shift due to the magnetic gradient pulses. But because the diffusion encoding magnetic gradient causes the field intensity to vary with spatial position, and if the proton has moved, it is subject to a different magnetic field strength during the second gradient pulse. This will lead to an overall phase shift because the second diffusion gradient pulse will not appropriately cancel out the phase shift caused by the first pulse. This phase difference is measured as a decrease in the amplitude of the perceived spin echo signal. The further away the proton has diffused, the larger the phase shift and the decrease in amplitude will be. [8, pp. 87–88] [9, pp. S210–S212] [11, pp. 161–164] The pulsed gradient spin echo sequence is visualized in figure 2.2.

Net magnetization is a vector sum of a large number of spin vectors, each in a different continuous motion. This causes phase incoherence and thus signal loss. The acquired signal in the presence of diffusion in an isotropic medium can be

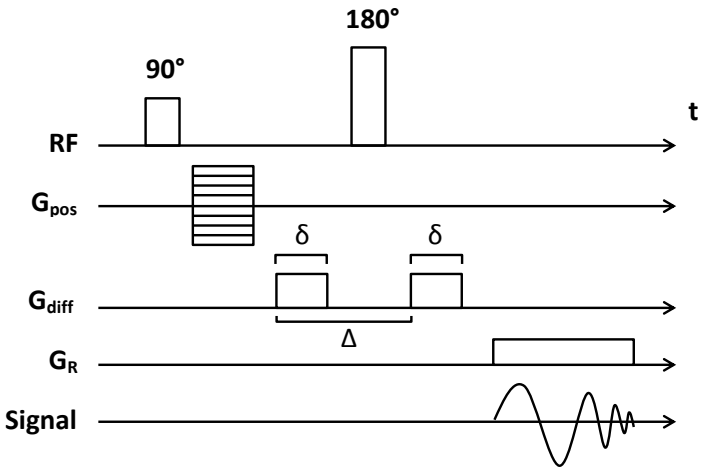

Figure 2.2: Pulse sequence diagram of a pulsed gradient spin-echo sequence used in diffusion MRI. RF indicates the given radio frequency pulses, G_{pos} is the position encoding magnetic gradient, G_{diff} refers to the diffusion gradient pulses, G_R is the signal readout gradient and Signal represents the acquired signal.

represented in the following manner:

$$S(b) = S_0 e^{-bM}, \tag{2.1}$$

where S_0 is the signal value without diffusion, M is apparent diffusion coefficient (ADC), representing the molecular diffusivity under motion restriction, and b is the diffusion weighting factor and can be defined as

$$b = \gamma^2 \delta^2 \left(\Delta - \frac{\delta}{3} \right) G^2. \tag{2.2}$$

Here γ is the gyromagnetic ratio of proton, δ is the duration of the two gradients, Δ is the time between application of the gradients and G is the amplitude of the diffusion gradients in PGSE. Diffusion weighting factor indicates the magnitude and duration of the applied field gradients and time between the paired gradients. Diffusion coefficient can be determined from a minimum of two different values of b and corresponding signal measurements, the values 0 and 1000 sec/mm^2 are often used. The measured diffusion coefficient is affected by several other movement sources like blood circulation in the microcapillaries, and therefore the term apparent diffusion coefficient is used. ADC maps are formed by calculating the apparent diffusion coefficient, M, for each pixel or voxel in the image by using equation 2.1 with predetermined and measured values for b, S_0 and $S(b)$. [8, pp. 87–88] [12] [13, p. 369]

2.3 Diffusion tensor imaging

For anisotropic media the diffusion distance is dependent on spatial orientation. When this directional dependency of ADC values is taken into consideration, the ADC value cannot be represented as a scalar anymore, and is replaced by a tensor. The form of imaging where instead of ADC, the corresponding tensor is acquired, is called diffusion tensor imaging (DTI).

A tensor can be simplified as a 3x3 symmetric matrix, and in the case of diffusion tensor imaging the diffusion coefficient M in equation 2.1 will be replaced with:

$$D = \begin{bmatrix} D_{xx} & D_{xy} & D_{xz} \\ D_{xy} & D_{yy} & D_{yz} \\ D_{zx} & D_{zy} & D_{zz} \end{bmatrix}, \tag{2.3}$$

where D_{xx}, D_{yy} and D_{zz} represent diffusion in the amount of the 3D coordinate system used for imaging. The matrix itself is a representation of an ellipsoidal isosurface presenting directional anisotropy of the matter through oriented diffusion. If we assume that the three diffusion eigenvectors, or the principal axes of the ellipsoid, are oriented along the axes of the used 3D coordinate system, equation 2.3 becomes

$$D = \Lambda = \begin{bmatrix} \lambda_1 & 0 & 0 \\ 0 & \lambda_2 & 0 \\ 0 & 0 & \lambda_3 \end{bmatrix}. \tag{2.4}$$

With equations 2.3 and 2.4 we can write

$$D = Q \times \Lambda \times Q^T, \tag{2.5}$$

where $Q = [\mathbf{q_1}\mathbf{q_2}\mathbf{q_3}]$ is the 3x3 matrix of eigenvectors $\mathbf{q_k}$ of D and Λ is the diagonal matrix with corresponding eigenvalues λ_k. [8, pp. 88–89] [12] [14, pp. 534–535]

Now we can rewrite equation 2.1 for diffusion tensor imaging as:

$$S(b) = S_0 e^{-b\mathbf{g}^T D\mathbf{g}}, \tag{2.6}$$

where $\mathbf{g} = \mathbf{G}/|\mathbf{G}|$ is the normalized vector $\mathbf{G}$, that is the unit vector in the direction of the magnetic diffusion gradient. The diffusion weighting gradient, b now becomes

$$b = \gamma^2\delta^2\left(\Delta - \frac{\delta}{3}\right)|\mathbf{G}|^2. \tag{2.7}$$

The diffusion tensor D has six independent elements (six degrees of freedom) and thus at least six linearly independent directions need to be used in the imaging

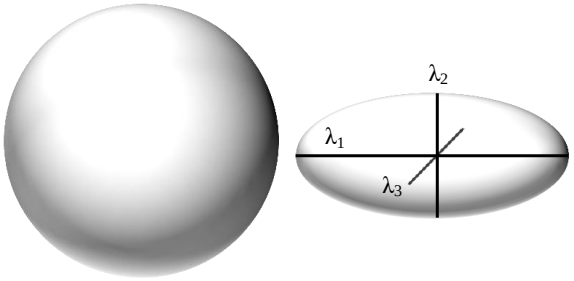

Figure 2.3: Diffusion presented with the help of ellipsoids; the circle on the left represents isotropic diffusion and the ellipsoid on the right represents anisotropic diffusion. Eigenvalues representing the strength of diffusion in different orthogonal directions are marked visible in the ellipsoid.

process along with the measurement without diffusion weighting, S_0. The apparent diffusion coefficient used as a measure in diffusion weighted imaging can be defined also simply as the average value of the measured eigenvalues

$$M = \frac{\lambda_1 + \lambda_2 + \lambda_3}{3}, \tag{2.8}$$

where $\lambda_1 > \lambda_2 > \lambda_3$. [8, pp. 87–88] [12]

Fractional anisotropy is a parameter most often used to describe the degree of anisotropic diffusion in white matter. The value of fractional anisotropy varies between zero and one, where the value one would represent a perfectly anisotropic diffusion and value zero represents isotropic diffusion. Fractional anisotropy is defined by the use of the measured eigenvalues:

$$FA = \frac{1}{\sqrt{2}} \frac{\sqrt{(\lambda_1 - \lambda_2)^2 + (\lambda_2 - \lambda_3)^2 + (\lambda_1 - \lambda_3)^2}}{\sqrt{\lambda_1^2 + \lambda_2^2 + \lambda_3^2}}. \tag{2.9}$$

Fractional anisotropy is a scalar quantity, but it is usually linked to the diffusion tensor when visualizing FA maps.

Visualization of FA is usually done by presenting FA as brightness and the direction of diffusion as hue, and an example of this kind of color representation is seen in figure 5.4. Diffusion tensor data can also be visualized by vectors or ellipsoids, where each voxel in the MR image is assigned either a vector displaying the direction and distance of diffusion or an ellipsoid constructed from the three eigenvalues λ_k. The ellipsoid's shape and thus the main direction of diffusion is dependent on the eigenvalues, i.e. strength of diffusion in each direction of the eigenvectors. Ellipsoids describing isotropic and anisotropic diffusion are visualized in figure 2.3, where on the left $\lambda_1 = \lambda_2 = \lambda_3$ and on the right $\lambda_1 > \lambda_2 > \lambda_3$. For clarification, the eigenvalue λ_1 is always the largest of the eigenvalues and is called axial diffusivity. Radial diffusivity is defined as average of the other two eigenvalues, λ_2 and λ_3. [8, p. 89]

3. MEDICAL BACKGROUND

In order to fully understand the concept of white matter neural tract analysis, diffusion and fractional anisotropy, basic knowledge of human brain anatomy and neural tract structure is required. A medical overview and an introduction to human brain atlas and white matter neural tracts is presented in this chapter. Human brain anatomy and structure will be briefly reviewed, followed by a short section on what neural tract analysis can do from a medical point of view.

3.1 Basic anatomy of human brain

Human brain can be divided in to four larger regions, starting from the spinal cord;

- The first structure is the brain stem, connecting the brain to the spinal cord.
- Second is the cerebellum (little brain), which is joined to other parts of the brain through the brain stem.
- Third is the diencephalon (interbrain), residing in between the brain stem and cerebrum.
- Fourth is the cerebrum, consisting of two nearly symmetric cerebral hemispheres.

These structures and locations of the different regions of the brain are shown in figure 3.1. Different type of brain segmentations are also used, and the brain can for example be divided into structural or functional segments [15, pp.75–78]. In figure 3.2 the brain and its different parts are segmented in a slightly more detailed manner. For most purposes the segmentation seen in figure 3.2 is sufficient, but white matter tract structure will be more thoroughly addressed.

In the lower part of the brain stem, resides medulla oblongata which connects the brain stem to the spinal cord. Pons is located near the center of the brain stem and connects the cerebellum to the cerebrum. The mesencephalon is located in the superior portion of the brain stem. The diencephalon consists of the thalamus, hypothalamus, epithalamus, pineal gland and pituitary gland. The cerebrum can be divided into frontal lobe, occipital lobe, parietal lobe and temporal lobe. The division of the cerebrum into different lobes is presented also in figure 3.1. In a simplified model the brain, and the whole central nervous system, can be divided

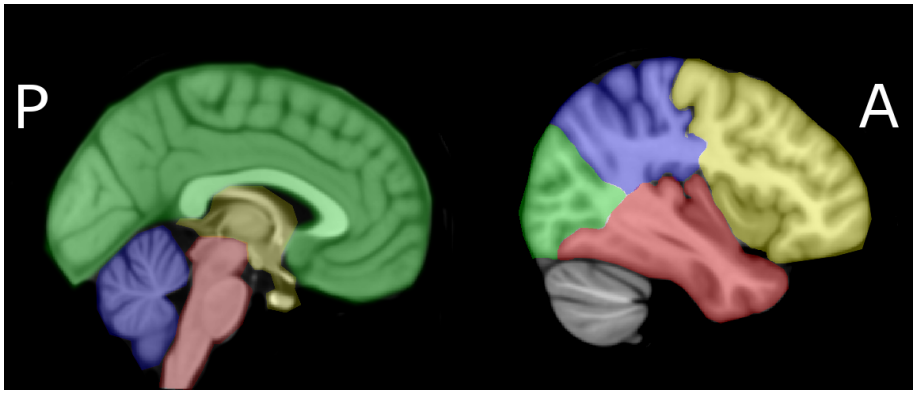

Figure 3.1: MRI derived visualization of the human brain and cerebrum segmentations with color highlighting. Left: brain stem is colored red, cerebellum is colored blue, diencephalon is colored yellow and cerebrum green. Right: frontal lobe is colored yellow, pariental lobe blue, temporal lobe red and occipital lobe is colored green, the cerebellum is also visible and uncolored. In the images, anterior side is on the right and posterior on the left.

into grey and white matter regions. White matter resides in the inner parts of the brain matter, and the outer parts of brain matter are of grey matter. In general the grey matter consists of somata and dendrites of the nerve cells, glial cells and capillaries. White matter contains mostly axons and glial cells. Because neural tracts reside mostly in the white matter areas, white matter will be more comprehensively addressed. [15]

3.2 White matter tract structure

Neural tracts are in fact myelinated axons, in which nerve impulses can propagate faster than in unmyelinated axons. The cerebral cortex is responsible for intellectual functions whereas white matter, in the inner parts of the cerebrum, provides connections between different areas of the brain and is thus an important part of brain functions [15]. The division of the cerebrum into grey and white matter is visualized in figure 3.3 by sagittal, coronal and transverse cross-sections of the brain.

White matter tracts can be classified into five categories according to their functions:

1. Tracts in the brainstem
2. Projection fibers (cortex-spinal cord, cortex-brainstem and cortex-thalamus connections)
3. Association fibers (cortex-cortex connections)
4. Limbic system tracts
5. Callosal fibers (right-left hemispheric connections, i.e. transverse fibers).

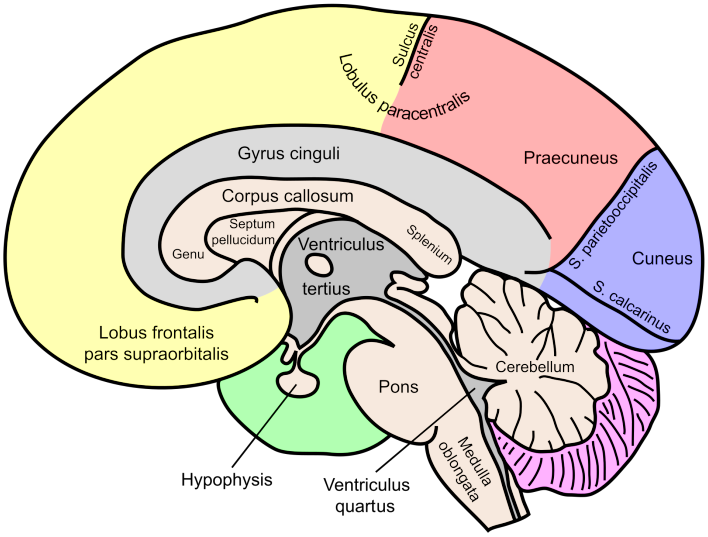

Figure 3.2: Human brain visualization with different structures named accordingly. [16]

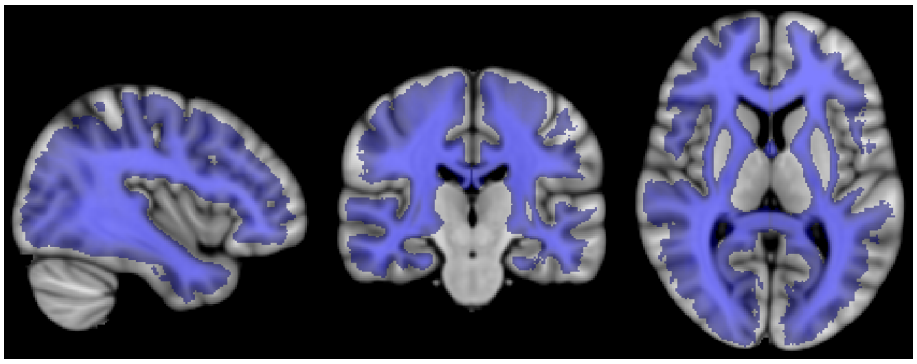

Figure 3.3: Cerebrum white matter probabilistic segmentation; blue color indicates areas which have a high probability of including white matter. Probabilistic white matter atlas presented here is based on Harvard-Oxford subcortical structural atlas. [1]

In the following subsections white matter tracts will be reviewed in their five corresponding categories and their visualizations by 3D tract reconstructions, acquired by means of continuous fiber tracking by Wakana et al. [17], will be presented. The neural tracts will also be presented in a 2D DTI colormap style for clarity.

Tracts in the brainstem

Brainstem white matter includes superior, middle and inferior cerebellar peduncles; corticospinal tract and medial lemniscus. Neural tract reconstruction of brainstem

[1] We are very grateful for the training data for FIRST, particularly to David Kennedy at the CMA, and also to: Christian Haselgrove, Centre for Morphometric Analysis, Harvard; Bruce Fischl, Martinos Center for Biomedical Imaging, MGH; Janis Breeze and Jean Frazier, Child and Adolescent Neuropsychiatric Research Program, Cambridge Health Alliance; Larry Seidman and Jill Goldstein, Department of Psychiatry of Harvard Medical School; Barry Kosofsky, Weill Cornell Medical Center.

fibers can be seen in appendix 1. The trajectory of superior cerebellar peduncle is somewhat flawed due to crossing fibers and in the reconstructed tract remains in the same hemisphere, although in fact it should cross to the other hemisphere. [17]

Projection fibers

Projection fiber tract reconstruction can be seen in appendix 2. The corticobulbar tract runs from various cortical areas to the brainstem. Projections from the corticospinal tract run towards pons (brain stem) and reach the pyramidal tract. Thalamic projections are clearly visible in the appendix 2, and they converge into the internal capsule. There may be some errors in the tract structures, particularly in microscopic crossing fibers, and this type of (diffusion MRI based) tract-tracking technique provides only macroscopic information on tract structures. [17]

Association fibers

Association fibers are shown in appendix 3. Although there are various types of association fibers: long range and short range cortical U fibers, the fibers shown in the appendix include only the most well-documented association tracts. The superior longitudinal fasciculus runs to the most lateral regions of the temporal lobe whereas the inferior longitudinal and inferior fronto-occipital fasciculi share projections at the posterior temporal and occipital lobes. The uncinate and inferior fronto-occipital fasciculi share projections at the frontal lobe. The only association fiber tract that runs medially to the thalamus and along the ventricle is the superior fronto-occipital fasciculus. [17]

Limbic system tracts

Cingulum, fornix and stria terminalis trajectories are reconstructed, along with hippocampus, amygdala and ventricles, in appendix 4. The cingulum collects tracts from nearby cingulate cyrus and extends up to the temporal lobe. The fornix projects into hypotahalamus, but is somewhat mixed with stria terminalis in the temporal lobe due to the reconstruction method and imaging resolution. [17]

Callosal fibers

Callosal fiber tracts are reconstructed in appendix 5. The vast amount of tracts run from the corpus callosum towards the cerebral cortex also form the corticocortical connections. Tracts from the genu of corpus callosum form the forceps minor and the tracts from the splenium form the forceps major. Projections that run inferiorly along the lateral ventricle from the splenium to the temporal lobes are known collectively as the tapetum. [17]

Transverse presentation

Appendix 7 includes the following brainstem tracts; corticospinal tract, medial lemniscus and superior and inferior cerebellar penducles. In addition to the tracts, the substantia nigra and deep cerebellar nuclei are identified. Some projection and callosal fibers can also be seen. The corticobulbar and corticospinal tracts are visible in the midbrain levels in the cerebral peduncle. The center portion of cerebral peduncle is filled by the corticospinal tract. The cingulum from limbic fibers is also visible in appendix 6. [17]

Thalamic fibers (radiations) join with corticobulbar and corticospinal tracts near the internal capsule, and can be seen in appendix 7. Tract near the lateral ventricle consists of superior longitudinal fasciculus, posterior region of the corona radiata and the callosal projection to the temporal lobe. The cingulum travels posterior to the splenium of corpus callosum and travels to the amygdala, and the fornix travels from the hypothalamic area, both of which can be seen in appendix 7. [17]

Some white matter areas are not classified in any of the tract families given here. An example of such area is the tract indicated by an asterisk in appendix 7; an area in the frontal white matter which consists of short range association fibers. Another similar area is indicated by a double asterisk in the occipital lobe. These tracts reside near the superior longitudinal fasciculus, and most probably are a part of it. [17]

3.3 Applications of neural tract analysis

Analysis of neural tract pathways through diffusion imaging has been a rising trend in medical neuroscience research field for some time now. Although not yet fully adapted for clinical use, DTI and neural tract analysis has been utilized in several different research projects concerning for example on axonal fiber connectivity [18], autism spectrum disorder [19], traumatic brain injuries [20] [21] [22] and even personality traits [23]. In general, white matter neural pathway tracking can be used to discover possible damage to the pathway structures, e.g. myelin sheets or other axonal structures, in the human brain. Analysis of white matter neural tract network is not a simple process, but a complicated ensemble of required steps to be taken in order to obtain the final results which can be used in the assessment of brain and neural tract network condition.

Water diffusivity is strongly linked to tissue pathophysiology, and information on tissue microstructure which otherwise could not be derived from T1 or T2 - weighted MR images can be derived through DTI. Many types of brain diseases cause structural changes in brain tissue which can be observed through diffusion imaging, by means of FA or ADC. Anisotropic diffusion is caused by different types

of ordered microstructures, which are present in white matter, muscle tissues, parts of the kidney and in the lens. Diffusion anisotropy in white matter is affected by several factors; fiber packing density, degree of myelination and fiber diameter. Thus lower than normal FA values in certain portions of white matter can be related to structural damage or decrease of the number of neural tracts. Lowered FA can for example originate from demyelination, decrease in fiber quantity or from any other type structural disparity of the fiber tracts. [24]

Myelin sheet damage or severe axon damage like broken tracts can be caused by various types of neurological conditions. A good example is multiple sclerosis (MS) where the myelin sheets around axons in white matter are damaged. Another, quite different example is traumatic brain injury (TBI), where the damage on white matter microstructure can occur almost anywhere in the brain. For TBI the damage is always different and individualized, thus group analysis and TBSS may give biased information when analyzing TBI patients. Because traumatic brain injuries are often hard to verify by other means of diagnosis than testing patients' cognitive functions, researchers are trying to link TBI to any structural changes in the brain. Due to the high prevalence of TBI, there is an acute need for a robust and accurate diagnosis method.

4. WHITE MATTER NEURAL TRACT ANALYSIS

Diffusion image data is originally in the form of 4D images containing at least one volume with no diffusion weighting ($b = 0$) and several diffusion weighted images taken with different gradient directions. Additional structural images may be included for registration purposes. These 4D images are of minimal use as such, but useful image modes like FA maps, ADC maps, tensor graphics and eigenvector and -value maps can be created by modifying and combining the diffusion images' information content. The FA maps are required for neural pathway analysis, from which the neural pathway structure can in theory be estimated in a quite intuitive, yet complex manner. The process of deriving the FA map and neural pathway data for analysis purposes is described in general in this chapter, and it is illustrated in figure 4.1. The diagram shows main phases of the pathway construction process, starting from the initial images and moving through preprocessing in the form of image modifications, and derivation of neural pathways, leading finally to the ready neural pathway data. Description of image acquisition step has been left out of the process due to its self-evident nature.

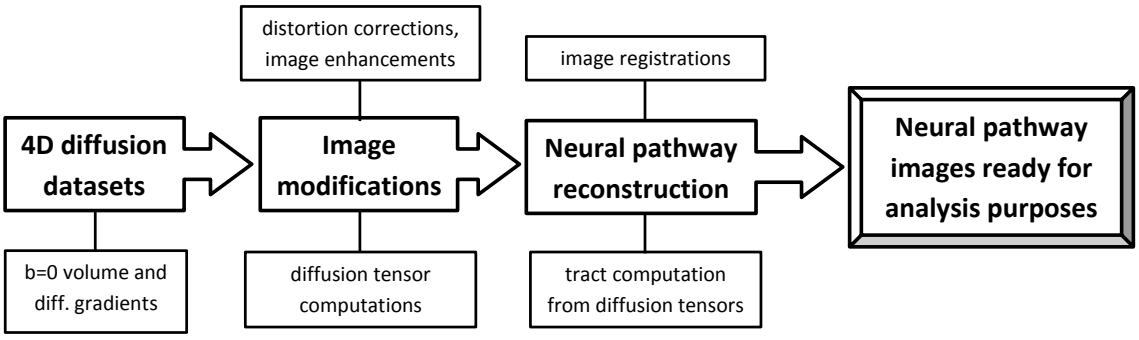

Figure 4.1: Different phases of the neural pathway image derivation process.

4.1 Image restoration and registration

Image restoration becomes even more important stage when analyzing more complicated medical images. For conventional radiographic images restoration is not as essential because the obtained images are often of sufficient quality for diagnosis or analysis as they are. For more complex cases like tomographic, perfusion and diffusion imaging, which usually include more significant artifacts, restoration is a

key point in producing adequate results. Major sources of artifacts in diffusion images include patient motion, eddy currents, noise and low acquisition resolution. In order to minimize these artifacts some image restoration methods are necessary. These methods include noise removal, sharpening and motion correction. There are also some precautions and equipment related procedures which can be applied to the image acquisition process that can reduce possible artifacts caused by patient motion and low acquisition resolution, but these methods are beyond the scope of this paper.

When enhancing or restoring digital images, the main component of the process is noise reduction; it is a vital part of restoration process because it is impossible to take a digital image without noise. In some applications noise reduction can be skipped, but it is then taken into account by some other means. Usually noise is reduced from digital images by smoothing or averaging the image picture element values. This may blur the image a bit, especially when using mean spatial filters, but the result will be more legible.

After noise reduction the image may still contain some spatial distortions caused by patient motion during the scan procedure. Diffusion images can also contain eddy current induced distortions. These aberrations are usually relatively easy to correct via linear registration. In some cases the images can be enhanced by adjusting their contrast, but when the absolute values of the picture elements are required, as is the case in DTI, adjusting the histogram in any way can result in data corruption. For optimal results, each voxel containing tissue information other than brain tissue should be removed from the images.

4.2 Neural tract derivation

The preprocessed diffusion images accompanied with tensor information per voxel are now ready to be analyzed for neural tracts, by a method called tractography. This is a quite intuitive stage, but nevertheless complicated algorithms are used to calculate probabilistic white matter neural tract directions. In principle neighboring voxels including directional and distance information of diffusion are now connected to each other to see if they are actually connected via neural tracts. [13]

Inference on neural tracts can be done in at least three different ways. One of the ways include a user set seed voxel or multiple voxels, also called a region of interest (ROI) based method, from which the used program then begins to calculate neural tracts propagating from. ROI based method usually does not find all the tracts in the brain, but is a good method if only a certain part of the brain or a certain fiber bundle is of interest. Using seed points in tractography is a heavily user dependent method with low repeatability. Another method for tractography is quantification of the probability of connectivity between two distant voxels. [13]

Third method for deriving white matter neural tracts involve only the use of FA maps instead of the whole tensor data. This method can only be used to derive the major tracts in white matter, but since it requires no ROI setting, it is much more repeatable and robust than ROI methods. The method includes skeletonising the areas of high FA, which presumably include multiple neural tracts. This method is described in detail in section 5.2. FA maps can also be used for ROI based methods by comparing FA values in areas of interest in an intersubject comparison.

5. FMRIB SOFTWARE LIBRARY

The software of interest is written mainly by members of The Oxford Centre for Functional MRI of the Brain (FMRIB) Analysis Group, and is freely distributed for non-commercial use from `http://www.fmrib.ox.ac.uk/fsl/`. The analysis software package as a whole is called FMRIB Software Library. FSL is not just a single program but rather a collection of different tools, subprograms, for different types of MR brain data analysis, designed to be used in a Linux based environment. The whole software package and its subprograms can be run on any Linux distribution, Mac OS X or on Windows PC via an emulation software. The software library also includes a subprogram called *FSLView*, an interactive display tool for 3D and 4D image data. The version of FSL used in this thesis is Release 4.1.9. [1] [2] FSL uses NiFTI-1 (Neuroimaging Informatics Technology Initiative) image data format by default, and although it can also work with ANALYZE^{TM}7.5, use of NiFTI format is recommended [25]. For the neural pathway analysis, analysis tool from the software library called Tract-Based Spatial Statistics is presented.

The software package's basic functions and tools are rather effortless to use. Unfortunately for the more advanced features the instructions on the website are either outdated or nonexistent. Thankfully there is an active forum from where answers for most of the questions about the software can be found, and the user base seems active enough if the user has a need to solve additional problems concerning the software. The message board can be found at `https://www.jiscmail.ac.uk/cgi-bin/webadmin?A0=FSL`.

5.1 User interface

FSL is a relatively user-friendly software, and it includes a graphical user interface (GUI) in addition to the command line utilities. In order to access the GUI one can open the Unix terminal and type in the command `fsl`, this will open the main GUI window. The GUI is made really simple, sufficiently easy to use and intuitive. Although a built in help guide would have been useful, the instructions and FAQ (Frequently Asked Questions) are available on the software's homepage, only one click away from the GUI. Additionally there are tooltip hints for most GUI elements, which are helpful. On the other hand, what is gained in simplicity is lost in practicality; the subprograms in GUI mode can only process one image at a time, and

some of the tools lack graphical interface entirely. The former would not be such a big issue with either small number of data or for single image analysis purposes, but most applications require at least dozens of images for accurate results, and going through them one by one is time consuming and cumbersome. There are some subprograms that are designed to be run only on one subject, and for these cases the GUI is more than an adequate environment. GUI of the software's main window and one of the subprograms, *Brain Extraction Tool*, is presented in figure 5.1. Not all of the tools included in FSL are implemented to the GUI, and they can only be accessed via their command line utilities.

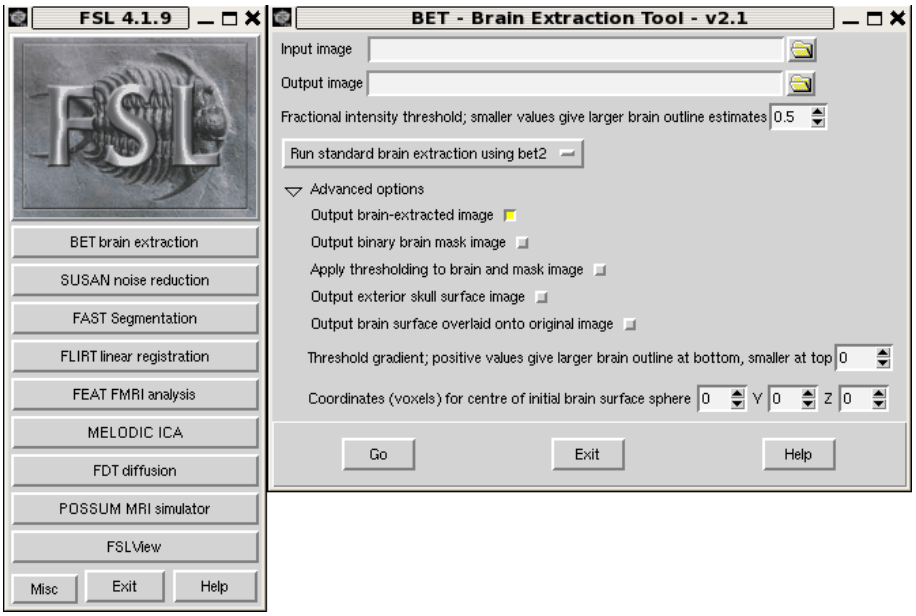

Figure 5.1: The graphical user interface of FSL main program with the brain extraction tool opened.

Whereas the GUI was easy and intuitive, the command line utilities are slightly more demanding but much more versatile. Because the command line utilities are accessed via the Unix shell, one can use bash commands to create customized scripts in order to, e.g., run several subprograms or process several images consecutively. While this requires some basic knowledge of the Unix environment, it can help make the analysis process smoother and improves its repeatability. All of the subprograms that are available through the GUI can also be run from the command line, along with the tools that do not have a GUI.

5.2 Neural pathway group analysis

Neural pathway structures in white matter can be modeled by taking advantage of fractional anisotropy data, and notable degradation of FA values in white matter is usually a sign of neural tissue damage. By comparing a group of subjects with

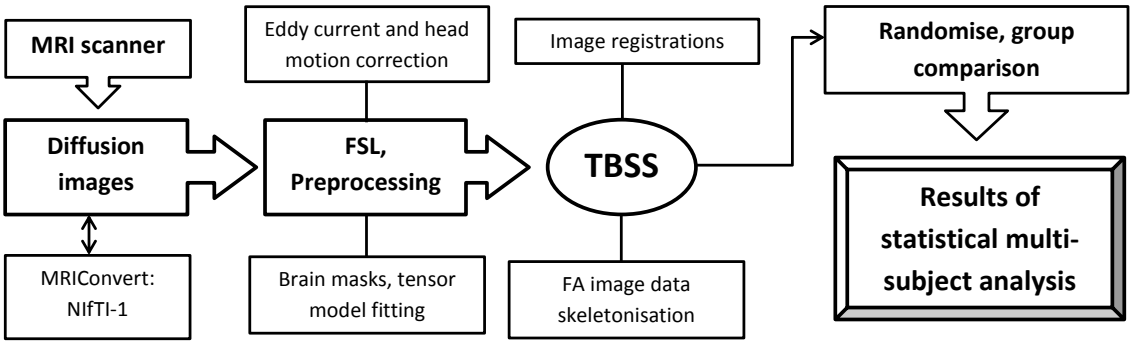

Figure 5.2: The procedure of white matter neural pathway analysis performed with FSL. The procedure is divided into four process stages depending on the type of tasks performed on the data at each stage.

any type of neural tissue degrading condition against a group of healthy control subjects, typical changes in the neural tracts can be determined for the condition in question. Although diffusion images can be used for single and multiple subject analysis, because TBSS is a multi-subject white matter neural tract analysis tool, it can be only used to analyze group differences. Let it only be pointed out that FSL does include tools for single subject neural fiber analysis, but this method will not be further addressed in this paper.

The procedure of checking two groups of subjects for differences in FA in white matter regions is reviewed in detail in this section. A mind map style image showing the basic phases of white matter neural pathway analysis conducted with FSL is presented in figure 5.2. Neural pathway information derived from FA data is constructed in the form of FA skeletons, which are, in theory, wire models of the main neural pathways in white matter. These skeletons will be used to statistically compare the FA values over white matter areas. FSL uses compressed NIfTI-1 format as default, but the user has control over the NIfTI format used by the programs.

5.2.1 MR brain images

Obviously the first stage of the analysis procedure is to acquire sufficient amount diffusion images (the more subjects, the more significant results) from a healthy control group and a group of patients one wishes to compare against the control group. An important issue to take into account is that in some cases, the resulting images from an MR scanner can be in a format which is not compatible with FSL, e.g. DICOM (Digital Imaging and Communications in Medicine) form. Because FSL uses NiFTI-1 data format by default, images in a different format should be converted into NIfTI.

Converting the images can be done with any desired conversion software. Many conversion software products are available on-line for free, but one of them is pre-

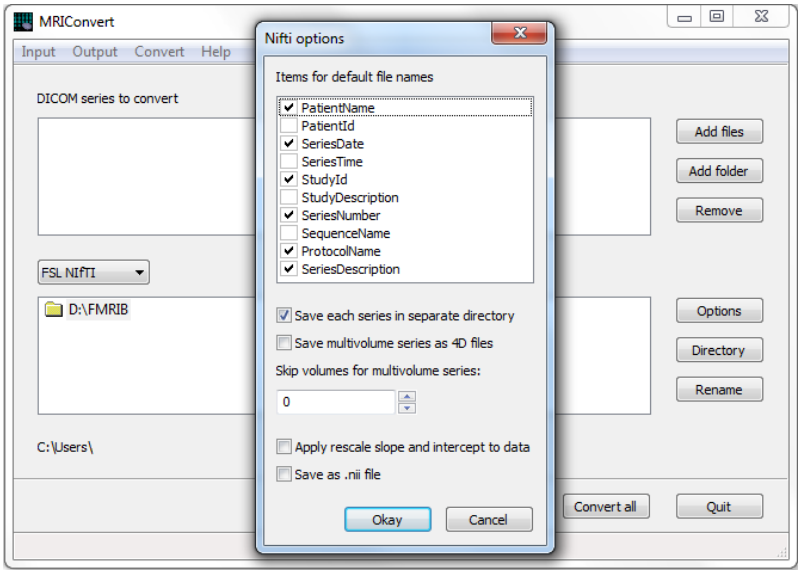

Figure 5.3: The user interface of MRIConvert with the options window opened.

sented here for the completeness of the process. A conversion software called *MRIConvert* [26] and its usage is presented shortly in this section. MRIConvert can convert DICOM files quite conveniently to NiFTI-1 format. Once you specify the location of your DICOM series, output directory for the converted images and set a few options, e.g. after what property are the files named after and how are multivolume series treated, the software effortlessly converts your data into the desired format. For TBSS purposes the **Save multivolume series as 4D files** and **Save as .nii file** options should be ticked. The GUI of MRIConvert is shown in figure 5.3.

5.2.2 Distortion artifact reduction

Artifacts arising from eddy currents and patient head motion are automatically corrected with a built-in software in FSL called *Eddy Current Correction*. The program corrects distortions caused by gradient coil eddy currents (first order linear image transformation) and simple head motion (rigid-body image motion) during scanning process by using affine registration to a selected reference volume. No spatial smoothing is applied to the images. [3]

Eddy current correction can be accessed both from terminal command and GUI. To run the tool via Unix shell, the following command should be used:

```
eddy_correct <input file> <output file> <reference No.>,
```

where `<input file>` is a 4D image file to be processed in NIfTI-1 or ANALYZE form, `<output file>` defines the filename of the output and `<reference No.>` states the reference volume to which all the other volumes in the 4D input file

will be registered to. The reference volume should be defined as the best MR image available for the data set. In practice the data set is a collection of 3D diffusion images collected with different gradient directions, and a T-weighted image or $b = 0$ (no diffusion weighting) volume is used as the reference volume. The GUI of the tool can be accessed by either running the command `Fdt` in the Unix shell, or alternatively `fsl` and opening the tool by clicking on the **FDT diffusion** button in the FSL GUI. After opening the FDT window, **Eddy current correction** can be selected from the drop down menu. Similarly to the shell command, the GUI asks for input, output and reference volume. Only one image can be processed at a time, but as mentioned earlier; shell scripts can be used to process several consecutive images automatically. Output of eddy current correction is the processed image with the specified filename.

5.2.3 Brain mask creation

Next phase in the group analysis with FSL involves the creation of binary brain mask images. The brain masks can be created with a subprogram called *Brain Extraction Tool* (BET) [27]. BET has various additional options for customizing the brain extraction process, but it can also be run by simply declaring the input and output files.

The tool itself can be accessed via its command-line script or through its GUI. Calling BET from the Unix shell is done with the following command:

```
bet <input file> <output file> <options>,
```

where `<options>` comprise the user chosen additional parameters which are used to customize the output of the brain extraction process. The option parameters available are described in table 5.1. Running the GUI version is done either by entering the command `Bet` or by selecting **BET brain extraction** from the main GUI. Input image, output image and fractional intensity threshold are needed to input for the brain extraction to run in the GUI. All the same options are available in the GUI version as in the shell version, and they can be found either from the drop down menu or under **Advanced options**. BET gives a stripped brain image as a default output, but it can be disabled. In the case of binary mask creation the output of BET is a binary 3D image file made from the input brain outlines, and is achieved by adding the option `-m`.

5.2.4 Diffusion tensor data compiling

Last phase of the actual image restoration, enhancement and modification prior to the TBSS analysis done with FSL consists of calculating the diffusion tensors from

Table 5.1: Option parameters available for BET. Parameters are inserted to the `<options>` part of the shell command. [27]

Parameter	Description
-o	Generates brain surface outline overlaid onto original image.
-m	Generates a binary brain mask.
-s	Generates a rough skull image.
-n	Does not generate the default brain image output.
-f <value>	Fractional intensity threshold (0–1); default=0.5. Smaller values give larger brain outline estimates.
-g <value>	Vertical gradient in fractional intensity threshold (-1 – 1); default=0. Positive values give larger brain outline at bottom.
-r <value>	Head radius in millimeters.
-c <x y z>	Center of gravity of initial mesh surface in millimeters.
-t	Applies thresholding to segmented brain image and mask.
-e	Generates brain surface as mesh in .vtk format.
-R	Runs a more "robust" brain center estimation: repeatedly calls the main program and attempts to find true center of gravity.
-S	Attempts to cleanup residual eye and optic nerve voxels which can sometimes remain after standard BET process.
-B	Attempts to reduce image bias and residual neck voxels.
-Z	This can improve brain extraction if only a few slices are present in the data(i.e., a small field of view in the Z direction).
-F	Uses BET to determine brain mask on the basis of the first volume in a 4D data set, and applies this to the whole data set.
-A	Generates skull and scalp surfaces in addition.
-A2 <value>	Same as -A, but a T2 image as input to improve skull and scalp feature extraction.

the raw diffusion data. This is achieved via a simple least squares fit of the tensor model to the diffusion data, after which the tensor eigenvalues and furthermore FA can be calculated [3]. The tool used for tensor calculation is called *DTIFIT*. DTIFIT requires the 4D image volumes, BET created binary masks, diffusion gradient directions (b-vectors) and diffusion weighting factors (b-values) for each corresponding image volumes in the 4D data. It is important that the order of entries in b-vector and b-value files are in the same order as the volumes in the input 4D image data set.

Diffusion tensor fitting tool, DTIFIT, can be run from both graphical and text-based user interfaces. The shell command for running DTIFIT is of the form:

```
dtifit -k <dti data file> -o <output basename> -m <binary mask file>
-r <b vectors file> -b <b values file> <options>,
```

where `<dti data file>` refers to eddy corrected 4D diffusion image file including

volumes with and without diffusion weighting, `<output basename>` is a user specified basename for naming DTIFIT outputs, `<binary mask file>` refers to the binary mask file of the input diffusion data created with BET, `<b vectors file>` refers the NIfTI file including gradient direction information, `<b values file>` refers to the NIfTI file containing b-values and `<options>` are optional arguments available for DTIFIT. The optional arguments are described in table 5.2. To use the GUI version of DTIFIT, either run `Fdt` or choose **FDT diffusion** from the main GUI, then choose **DTIFIT Reconstruct diffusion tensors** from the drop down menu. For the GUI version input required is either an input directory, or manually specified files (**Specify input files manually**) which contain the same data as the shell command input arguments. The directory input should be avoided since it requires all the inputs to have standardized filenames. The optional parameters in text based interface are not available in GUI version. As with other tools, usage of the Unix shell command is recommended over the GUI version due to its versatility.

DTIFIT generates multiple output files. The base outputs of DTIFIT are the following 3D images:

- Three eigenvector image files; 1st (<basename>_V1), 2nd (<basename>_V2) and 3rd eigenvectors (<basename>_V3).
- Three eigenvalue images, suffixes _L1, _L2, _L3.
- Mean diffusivity image, better known as Apparent Diffusion Coefficient (ADC) map (_MD).
- Fractional anisotropy, suffix _FA.
- Mode of anisotropy (suffix _MO) with scale: oblate=-1, isotropic=0, prolate=1.
- Raw T2 image with no diffusion weighting, suffix _S0.

The first eigenvector image can be viewed as a color coded diffusion map, where different directions of the vector are coded with different colors. An example of this can be seen in figure 5.4. For TBSS purposes the most interesting image is the fractional anisotropy image, although, for example ADC maps can also be compared in a similar manner as FA images.

5.2.5 Preprocessing

Before the images are aligned and registered there is a small preprocessing step to be taken. This is the first actual step of the TBSS procedure. Before running this preprocessing phase, the FA files created in the previous phase need to be copied

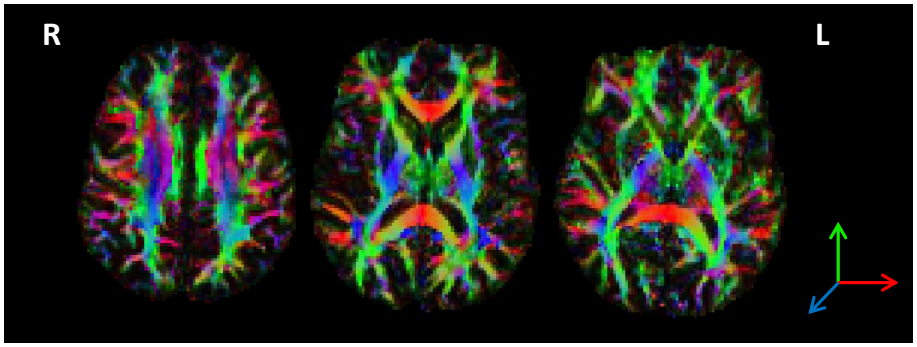

Figure 5.4: Color coded fractional anisotropy map. Different colors represent the primary directions of diffusion: red, left-right; blue, superior - inferior ; green, anterior - posterior.

Table 5.2: Optional parameters available for DTIFIT. Parameters are inserted to the `<options>` part of the shell command. The program can be run without any of the parameters listed here.

Parameter	**Description**
-V	Switches on diagnostic messages.
-h	Displays help message (same as running with no arguments).
--cni	Input confound regressors.
--sse	Output sum of squared errors.
-w	Fits the tensor with weighted least squares.
--littlebit	Only process small area of the brain.
--save_tensor	Saves the elements of the tensor.
-x	Minimum value of x.
-X	Maximum value of x.
-y	Minimum value of y.
-Y	Maximum value of y.
-z	Minimum value of z.
-Z	Maximum value of z.

to a new folder where they will be processed. The images should also be renamed accordingly; the two groups, control and patient groups, should be separated from each other. This is done so that the images belonging to the different image sets are alphabetically separated from each other, and can be differentiated later on. For example the files could be renamed so that the control group images would be listed before patient group images by adding prefix "CON" to control group and "PAT" to patient group files, so that the control data is before the patient data alphabetically. This is also a necessary step for the statistical comparison of the two groups.

After the image files have been renamed, the actual TBSS preprocessing phase may be run. The script needs to be run in the folder where the FA images are copied, and is done by running the command

```
tbss_1_preproc *.nii.gz.
```

This processes all the NIfTI images in the folder and places the results into a new subdirectory called `FA` and the original FA files to a directory `origdata`. The script first erodes the FA images slightly and sets all voxel values in the end slices zero. This removes possible outliers caused by tensor fitting process. The script also runs another subprogram, `slicesdir`, which creates a simple web page including a static view of each of the input FA images. These can be checked by the user for any prominent errors in the image data. After deeming the images correct, the next phase of the process can be started. There is no GUI available for the tool used in preprocessing stage, nor in any of the following stages. Only exception is a tool used for generating general linear model (GLM) matrices for the statistical group wise analysis, but more information on the tool itself can be found later on.

5.2.6 Image alignment

Image alignment phase is divided into two different parts; first an affine registration is performed between the images to gain initial alignment. After this a voxelwise nonlinear registration with intermediate degrees of freedom (DoF) is performed on the images in order to align the images sufficiently well for the skeletonization stage. The DoF cannot be too low in order to succeed in the intersubject alignment for white matter tracts, but DoF cannot be too high either in order to keep the neural pathway structure intact and to register correct corresponding tracts to each other. The nonlinear registration approach used by TBSS is based on free-form deformations and B-Splines. The objective is to preserve overall structural topology in the alignment, but still align the data sufficiently to allow direct comparison. [3]

There are three different ways to complete the nonlinear registration:

1. Registering the FA images to a the FMRIB58_FA standard-space image, an averaged FA map included with the software package,
2. registering the FA images to a user defined target image
3. or by identifying the "most representative" target from the FA images and using it as a target image.

The first option is generally recommended; it usually gives good results and it involves only one registration per subject. Second option also involves only one registration but requires a user-defined reference image as input. If the study group differs somehow from a "generic" group of subjects, e.g. in the case of studying young children, the adult derived FMRIB58_FA image might be unsuitable and either of the two latter options should be used. The third option compares all the subjects' FA images against each other and determines the subject which requires least amount of warping when used as a target for registration [3]. The method

requires the registration of each subject to every other subjects, resulting in a much longer runtime than the two former methods when processing even marginally larger group sizes.

Independent of which method is chosen, all the images will be affine-aligned to MNI (Montreal Neurological Institute) 152 1x1x1mm^3 standard space, which has been deemed the most convenient solution based on interpretation, display and analysis results. Working in higher resolution space prevents further partial volume effects, although it increases the computation time slightly. The affine and nonlinear registrations are combined in order to avoid resampling the images twice. [3]

The mentioned image registrations are performed by running the following script in the same folder (which includes the subfolders `FA` and `origdata`) as the command from previous stage:

```
tbss_2_reg <option>,
```

where `<option>` is either `-T` for using FMRIB58_FA as the registration target, `-t <imagefile>` for using a user defined target or `-n` for identifying the most representative target and using it as the registration target image. The script processes FA images in the folder `FA`, and no visible results will be produced from this stage. The next phase can be began after the registrations are completed.

5.2.7 Fractional anisotropy skeletonization

In this phase all the aligned FA images are first combined into a single 4D image including the subject images as time series points. Next the images are averaged in order to create a mean FA image. The average FA image represents the FA values common in the whole study population, i.e., the areas with the highest degrees of FA values common to all (or most) subjects are shown in the image as brighter areas. No smoothing is applied to the mean FA image because the image will be natively spatially smooth due to the upsampling and averaging. The mean FA image is then used to derive a mean FA skeleton, which should represent the location of major neural tracts shared by each subject.

The skeleton is a one voxel thick structure running through the main neural pathways in white matter. Several parts of the skeleton may seem like thicker than one voxel, but it is only due to its 3D nature; fiber bundle surfaces parallel to the viewing plane seem thicker than one voxel. According to Smith et al. [3] white matter tracts can be simplified to two different structures: curved sheets of a certain thickness or curved tubes. These structures can be represented accordingly as a thin curved surface or a thin curved line running through the middle of the fiber bundle.

In the skeletonization process, first the directions perpendicular to the fiber bundle directions are determined by using local FA center of gravity in a 3x3x3 voxel

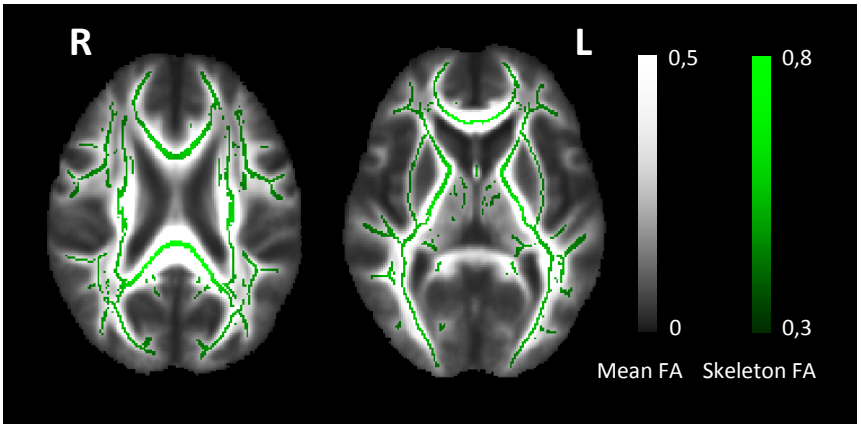

Figure 5.5: Mean FA image shown in greyscale image with mean FA skeleton overlaid on top (green).

neighborhood (i.e. examining the first derivative of the image). The vector running from the center of the 3x3x3 neighborhood to the neighborhood's FA center of gravity should point towards the tract center, and thus show the direction perpendicular to the tract. This way the directions perpendicular to the local tract structure are formed throughout the volume. The process is done only for voxels with FA values not close to zero. Second derivative of the FA image is used to find the remaining perpendicular directions. When the perpendiculars are found, all the direction estimates are replaced with modes of quantized local 3x3x3 set of estimated directions in order to make the perpendiculars more coherent. [3]

With the perpendiculars defined, the skeleton itself can now be prepared. For each voxel its FA value is compared with two closest neighbors in the tract perpendicular direction, and if the value is larger than both of the neighboring voxels, the voxel in question is marked as lying on the skeleton. Repeating this for the whole image results in a FA skeleton that represents white matter neural tract structures in the mean FA image. The skeleton should be thresholded in order to remove areas subject to possible large intersubject variations (utmost edges of the cortex) and areas which are primarily cerebrospinal fluid or grey matter. A good FA value for thresholding according to Smith et al. [3] is between 0.2 and 0.3. The excluded areas of the skeleton would most likely not correspond well with tract structures across subjects. An example of a FA skeleton derived from multiple subjects is shown in figure 5.5.

The skeleton may have gaps and disconnections in its tract structures, and this is mainly because of crossing fibers. The perpendicular direction is not well defined in junctions, which disturbs the perpendicular designation process. Also the fractional anisotropy value of a voxel containing crossing fibers may appear low due to summing of the multiple tracts and their fractional anisotropies.

All of the above, combining the FA images to a single 4D image, creating the

mean FA image and mean FA skeleton is done with a single command

```
tbss_3_postreg <option>,
```

where `<option>` is either `-S` for deriving the mean FA image and mean FA skeleton from the study subjects, or `-T` if the user prefers to use FMRIB58_FA and the skeleton derived from it in the study. The former option is recommended. After this stage the mean FA image and the skeleton will be placed in a subfolder `stats`. The skeleton should be viewed (e.g. in FSLView) at this time in order to check a suitable threshold value for cropping smaller FA valued areas. For example, if the user wishes to view the mean skeleton on top of each FA image separately, it can be by entering the following command in the `stats` directory:

```
fslview all_FA -b 0,0.8 mean_FA_skeleton -b 0.2,0.8 -l Green.
```

This will display the 4D image of all the subjects' FA images below the mean FA skeleton. The threshold can be changed inside FSLView in order to determine the best value, which will then be used in the next phase.

5.2.8 Fractional anisotropy value projection

Now that the mean FA skeleton is ready, a FA skeleton needs to be created for each subject. This is done by "projecting" the FA values of each subject's tract centers to the mean skeleton map. Projecting the values of FA from the tract centers to the mean skeleton is accurate even if there is some extent of misalignment between the subjects after the nonlinear registrations. It is the skeletonization and FA projection method which makes perfect alignment during the whole TBSS process unnecessary.

For each voxel in the skeleton a corresponding maximum value in the perpendicular direction is searched from the subject's FA image. Note that the perpendicular directions are already computed with the formation of the mean FA skeleton. The maximum FA value is then assigned to the skeleton voxel in question. This approach accomplishes accurate alignment in the tract perpendicular direction across subjects, but not parallel to the tract. Because FA changes are more dramatic in the perpendicular direction than in parallel direction, this type of solution benefits the analysis greatly.

Two constraints are placed for the search process; first the search of maximum FA value is limited to a distance from the voxel that is closer to the starting section of the skeleton than any other section of the skeleton. For this purpose a skeleton distance map is created, which effectively shows the distance of each voxel from the nearest skeleton voxel. The constraint also ensures that every voxel in the image is mapped only to a single point in the skeleton: the maximum FA value search, starting from a voxel in the skeleton and continuing outwards from the skeleton, can

continue only while the distance value is increasing. An example of a distance map used in the projection process is shown in figure 5.6.

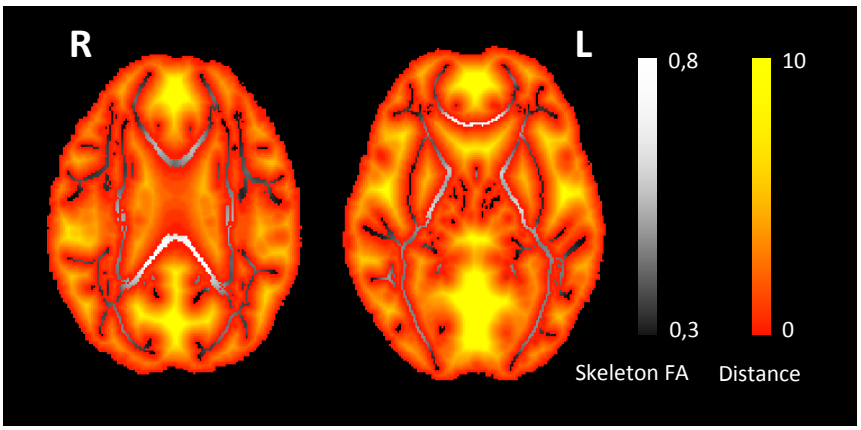

Figure 5.6: A distance map used in the FA value projection to the skeleton. Mean skeleton can be seen underneath the distance map where the distance is marked as zero.

The second constraint is a soft distance limit placed on the maximum search distance. A wide Gaussian function (FWHM 20mm) is applied as a weighting function to FA values when searching for maximum FA. The function deweights the most distant voxels in the search and effectively emphasizes the nearby FA values. After finding the voxel containing the maximum value, its original value is then placed to the skeleton voxel.

The Unix shell command script used in this step requires the threshold determined in the end of last phase as an input. The mean FA skeleton will be cropped of all the values under the given threshold and only afterwards used for the projection. The script for this phase is as follows:

```
tbss_4_prestats <threshold>,
```

where `<threshold>` is the chosen FA threshold value for the skeleton. This script creates the distance map after cropping the mean skeleton, projects all the subjects' FA images to the skeleton and creates a 4D image containing the FA skeletons for each subject. This file (`all_FA_skeletonised`) will be fed to the voxelwise statistical analysis in the last phase of TBSS.

5.2.9 Inference

In the last phase of the TBSS analysis a statistical comparison between the created FA skeletons of the two groups is conducted. The subjects' FA images are now fully aligned through skeletonization process and are thus ready for direct comparison. The comparison is done by utilizing univariate linear modeling; applying multiple regression across subjects. For finding differences between two groups, an unpaired

t-test is applied in order to test statistically significant local differences between the two groups. The FA value data distribution in the skeletons are of Gaussian form, and simple parametric regression and inference can be deemed valid.

The multi-subject (group) comparison is done by using a multiple comparisons permutation test approach addressed by Nichols and Holmes [28], by testing for example voxel t-value or cluster size against the null distribution of maximum values of the test statistic. The null distribution in general in this type of problems is unknown, and thus generated by random permutations of the subject ID. This type of approach gives good control over the probability of falsely rejecting a voxel hypothesis. Using a permutation based approach actually does not require the cross-subject FA distributions to be of Gaussian form.

Creating the needed GLM files

For TBSS group comparisons the use of Randomise requires a GLM design matrix and t contrasts as inputs, which inform the program of number of groups, which subjects belong to which group, which statistical properties are tested and how they are compared, and possible covariates (age, gender, etc.). There are three different ways to create the design files (matrix and contrasts):

1. running the GUI for designing GLM:s via the command `Glm`,
2. manually editing the matrix and contrast files prior to running Randomise,
3. or by using the shell command `design_ttest2` to create the files for a simple two group unpaired t-test.

The first and second options are quite equal when considering the outcome, but the third option should be only used for age matched two group comparisons.

The GUI version can also be run from the main GUI by choosing **Misc** and **GLM Setup**. Running the tool, either from Unix shell or from the FLS main program, opens two separate windows. The **GLM Setup** window is first used to select **Higher-level / non-timeseries design** from the dropdown menu. Then the amount of subjects should be defined in the **# inputs** box and the button **Wizard** chosen from the window. This will open a new window from which the **two groups, unpaired** should be selected and the number of subjects in the first group entered for the two group TBSS analysis purposes. Clicking on **Process** will change the **General Linear Model** window accordingly and present a graphical view of the model.

Amount of subjects and to which group they belong can be seen and edited in the **EVs** tab. For the case of two groups the **EV1** and **EV2** represent the two different groups and their values should be set to **1** for subjects belonging to the

corresponding group. Subjects in groups 1 and 2 are determined by alphabetical order of the FA filenames. For example using the prefixes "CON" and "PAT" for controls and patients respectively would make group 1 control group and group 2 patient group. Possible covariates can be added in this tab also, and age has been added as a covariate as an example in figure 5.7. The covariates need to be demeaned in order for them to work, that is the average value needs to be deducted from each value in order to make zero as the mean value of the covariate. The added covariates are taken into account in a linear manner when the statistical comparisons are made.

Different tests to be performed can be chosen via test contrasts from the **Contrasts & F-tests** tab. For example the tests in the figure 5.7 include the differences between FA values in group 1 and 2 (C1, group 1 FA > group 2 FA; C2, group 1 FA < group 2 FA) and mean values for both groups (C3 and C4). The values in **EV3** and higher (covariates) should be kept zero due to the demeaning of the input values. For TBSS the differences between the two groups are the only needed contrasts, and the group means can be disabled. Group differences and mean values are added to the contrasts automatically by the GUI program.

Editing the design files with a text editor is a more challenging task but can be faster when used appropriately. An example of both design matrix and contrast file is shown in figure 5.8. Easiest way to create the design files by hand is to first create the simple two group unpaired t-test files by using the method described by the third option; `design_ttest2 <basename> <#_G1> <#_G2>`, where `basename` is the name used for the matrix and contrast files, `<#_G1>` is the amount of subjects in group 1 and `<#_G2>` is the amount of subjects in group 2. The command results in design matrix and contrasts file for a simple two group difference comparison without any covariates. The generated design files need to be in the same folder with the FA skeleton data (`stats` directory).

Running permutation tests

With both design matrix and t contrasts files ready, the permutation tests can now be run by executing a program called *Randomise*, a simple permutation tool for modeling and inference using GLM design setup. The program is run by executing the following shell script in the `stats` directory:

```
randomise -i <input> -o <output> -m mean_FA_skeleton_mask -d
<design.mat> -t <design.con> <options>.
```

Compulsory arguments for TBSS group comparison are `-i <input>`, `-o <output>`, `-d <mat>` and `-t <cont>`, where `<input>` is the 4D image file containing all the subjects' skeletons (`all_FA_skeletonised` for FA comparison), `<output>` is a user defined output file basename (if only FA values are compared, this can be set to

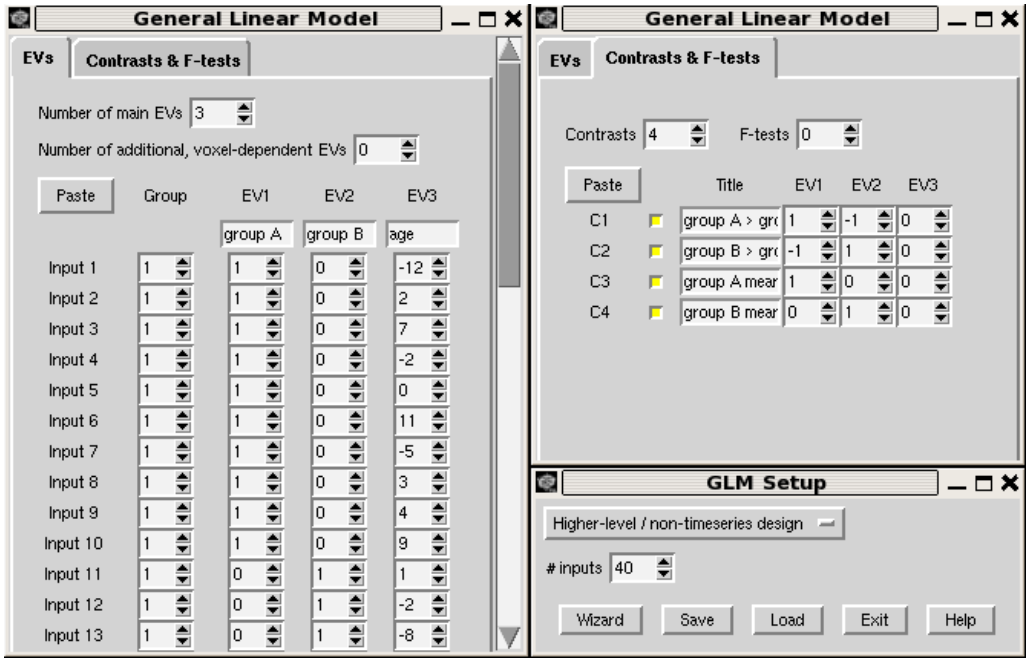

Figure 5.7: General Linear Model GUI. Both "EVs" and "Contrasts & F-tests" tabs are visible, and in this case the first 10 subject of a total of 40 belong to first group and the rest to the second. Demeaned age values are added as a covariate and four different contrasts are determined: group 1 FA> group 2 FA, group 1 FA < group 2 FA, group 1 mean values and group 2 mean values. Note that groups are named A and B in the GUI instead of 1 and 2.

e.g. `tbss`), `-m mean_FA_skeleton_mask` feeds the thresholded skeleton area to the program, `-d <design.mat>` is the filename of created design matrix file and `-t <design.con>` is the filename of the created t contrasts file. All the other inputs are inserted after design contrasts file to `<options>`, and a full list of options is found in appendix 8.

There are a couple of different ways to how the program does its thresholding in the group comparison, which also effect on the output of the program. The following options for thresholding are available:

- Voxel-based thresholding, both uncorrected and corrected for multiple comparisons by using the null distribution of the maximum voxelwise test statistic. It is applied by using `-x` in the `<options>` for Randomise.

- Threshold-Free Cluster Enhancement (TFCE), a new method for finding clusters in the data without having to define the cluster size in advance. TFCE is applied by `-T` for normal 3D data, and for TBSS analyse `--T2`.

- Cluster-based thresholding corrected for multiple comparisons by using the null distribution of the maximum cluster size. This option is applied by `-c <thresh>` for t contrasts and `-F <thresh>` for F contrasts.

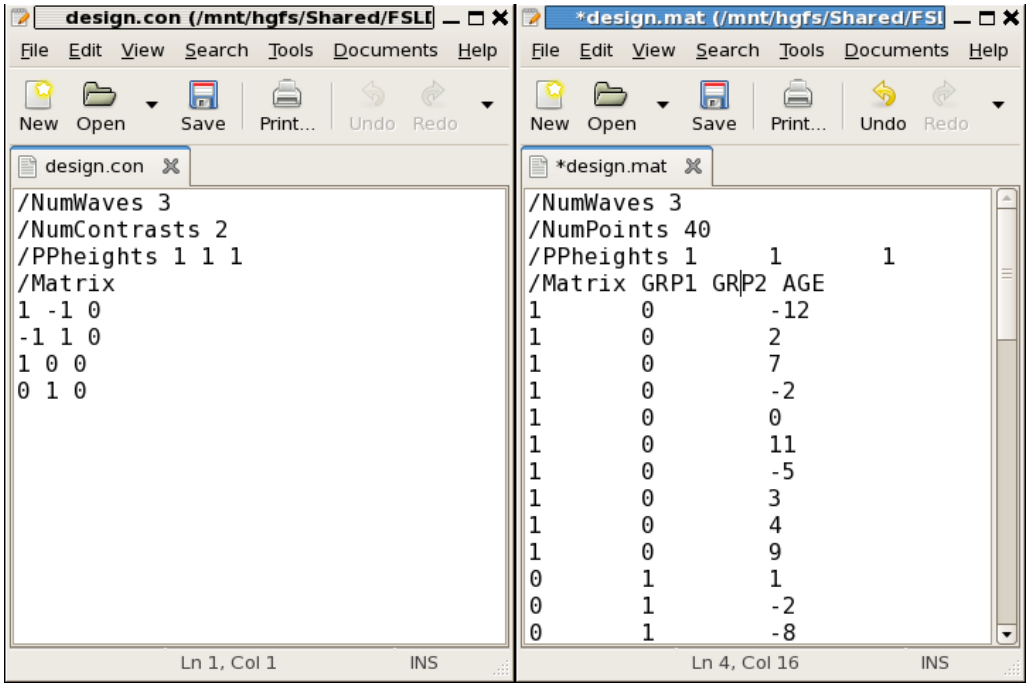

Figure 5.8: Similar GLM contrasts file and design matrix to the one presented in figure 5.7, created with a text editor.

- Cluster-based thresholding corrected for multiple comparisons by using the null distribution of the maximum cluster mass. It is applied by `-C <thresh>` or `-S <thresh>` for t or F contrasts.

Output names of the different thresholding options are listed in table 5.3 for voxelwise and TFCE and in table 5.4 for clusterwise option.

Table 5.3: Output filename extension of voxelwise and TFCE thresholding in Randomise.

	Voxelwise	**TFCE**
Raw test statistics	`_tstat` `_fstat`	`_tfce_tstat` `_tfce_tstat`
1 - uncorrected p	`_vox_p_tstat` `_vox_p_fstat`	`_tfce_p_tstat` `_tfce_p_fstat`
1 - FWE corrected p	`_vox_corrp_tstat` `_vox_corrp_fstat`	`_tfce_corrp_tstat` `_tfce_corrp_fstat`

The TFCE approach on thresholding is a new technique designed to improve cluster based thresholding. Cluster based thresholding is more sensitive to finding real signals than voxelwise thresholding, but the drawback is the need for an initial value of a cluster-forming threshold, which has a large impact on the results. TFCE is a method which enhances local clusters, making them more easy to detect. The method is usually as sensitive as cluster-based methods and more robust. The output of TFCE can be changed into voxelwise p-values. [29]

Table 5.4: Output filename extension of clusterwise thresholding in Randomise.

	Clusterwise	
	Size	**Mass**
1 - FWE corrected p	`_clustere_corrp_tstat` `_clustere_corrp_fstat`	`_clusterm_corrp_tstat_` `_clusterm_corrp_fstat_`

The output images are, with the exception of raw test statistics, $1-p$ images where value 1 is the most significant. These images should thus be thresholded for viewing at range $1-p$, that is if statistically significant results are wanted, the image should be thresholded at >0.95. FWE corrected means that familywise error rate is controlled. For a FWE corrected image with thresholding at p<0.05, the chance of one or more false positives in the image is 5%, also the chance of having no false positives is 95%. The results are also numbered, and for example the file `tbss_tfce_corrp_tstat1` gives familywise corrected TFCE results where group 1 has larger voxel values than group 2. That is, in the case of FA images the areas of the skeleton where group 1 has statistically larger FA values are visible in the resulting images. Group 1 is the group consisting of data with filenames that come first in alphabetical order. If the naming is done with prefixes CON and PAT for control and patient data, contrast 1 would be the results of control>patient test, and contrast 2 would be the results of control<patient test. In the case of more complex contrasts, the numbering of the results can be discovered from the order of the contrasts defined in the contrasts file.

Deriving quantitative data

Although most of the inference is in qualitative form (images consisting of statistically significant areas with differing FA values), some quantitative results may also be obtained after the TBSS process. Obtaining for example cluster sizes, positions of maximums and centers of gravity of the significant clusters is a really straightforward operation, and can be done with a single command

```
cluster -in=<filename> -thresh=<value> <options>,
```

where `<filename>` is the result of TBSS to be examined, for example the file for FWE corrected contrast 1 TFCE output `tbss_tfce_corrp_tstat1`, and `<value>` is a desired threshold for cluster significance $1-p$, for example 0.95 or higher. Additional options and arguments for the program is input to `<options>`, and a list of available options can be seen from appendix 9. The program output is a table with cluster information by default, and additional outputs like a cluster map can be defined through the additional options.

In order to obtain FA values of the clusters one first needs to create binary masks from the significant clusters reported by the cluster program. The option `-oindex` will create an image file with the significant cluster volumes marked with their corresponding cluster index. This file needs to be then divided into separate cluster mask images by using *fslmaths* subprogram for each of the found clusters. Separating the clusters with fslmaths can be done with the following command

```
fslmaths <clusterfile> -thr n -uthr n -bin <clustermask>,
```

where `<clusterfile>` is the output of indexed clusters created with cluster, `n` is the index of the current cluster and `<clustermask>` is a user defined output name for the binary cluster mask. The command needs to be run for each cluster, changing `n` and `<clustermask>` for each cluster. Fslmaths has countless other uses, but they will not be addressed here.

Now the average FA values for each subject in a selected cluster can be derived with the command

```
fslmeants -i all_FA_skeletonised.nii.gz -o <data_n> -m <cmask_n>,
```

where `<data_n>` is the output filename of n:th cluster data and `<cmask_n>` is the cluster mask created earlier for the n:th cluster. The outputs of fslmeants are text files containing average FA values of the cluster in question from each subject. The file only contains the values, and they are in the same alphabetical order as discussed earlier. This data can then be used for example to calculate the mean FA and standard deviation in significant clusters for both groups.

Using non-FA images in TBSS

TBSS can also be used for analysis of other than FA images, for example ADC map group comparison may be of interest. It is recommended to use the already derived FA data for the registration and skeletonization stages. First the standard TBSS procedure with FA data should be run in its entirety. Now a new folder should be created in the working directory of TBSS, including `origdata`, `stats` and `FA` directories. The folder's name can be anything user defined, for example `ADC`. Depending on which diffusion derived data is wanted for the analysis, the corresponding data should be copied to the new folder. The data to be copied is at the folder including the results from DTIFIT. Any of the results (see section 5.2.4) can be used for the group analysis. After copying the data, it needs to be renamed; the data needs to be named *exactly* the same as the original FA data, including the suffixes. The original filenames can be checked from the `origdata` folder.

After renaming the files the alternative TBSS script can be run. This is done by running the following command in the TBSS working directory:

```
tbss_non_FA <alternative-image-rootname>,
```

where `<alternative-image-rootname>` is the name of the folder. The name input to the program will be used to name the output files. For the sake of example, the input alternative root name is assumed to be *ADC*. Running the script applies the original registration to the data, merges the images to a single 4D file, `all_ADC`, and projects the data into the mean FA skeleton, creating `all_ADC_skeletonised`. Now the voxelwise statistics can be run on the `all_ADC_skeletonised` in the same manner as previously described for FA images.

5.2.10 Viewing the qualitative results

Now that the whole TBSS process is finished, the results can be examined. This can be done with any image display tool, but FSL has an interactive display tool, *FSLView*, and its utilization will be described. The results are usually displayed as three layers of images: the mean FA image as a background, FA skeleton on top of it and the statistics image overlaid on top of both. Easiest way to accomplish this is to run the following command in the `stats` directory:

```
fslview mean_FA mean_FA_skeleton -l Green -b 0.3,0.8
<stats> -l Red-Yellow -b <p-value>,1 .
```

Here `<stats>` is a desired thresholding statistics result, e.g. `tbss_tfce_corrp_tstat1`, and `<p-value>` is the desired confidence value, which for statistically significant results it should be at least `0.95`.

The results can also be viewed by opening FSLView via the main GUI or by running the command `fslview`, and manually opening the image files in the following order: mean FA, mean skeleton and TBSS statistics file. The mean skeleton should be thresholded at [0.3–0.8]; the lower limit is the same value as was used for thresholding the mean skeleton image and the upper limit is purely due to convenience of display.

5.3 Other features

FSL is abundant of features when it comes to MR image processing; there are tools for comprehensive functional, structural and diffusion MRI analysis as well as some accessory tools. All of the subprograms included in the software library are listed in this thesis, but only some of the tools are more thoroughly addressed. Review of each tool in the FMRIB Software Library is out of the scope of this paper.

Subprograms are divided into four different categories and subsections according to their usage; structural MRI, functional MRI, diffusion MRI and other tools. The complete list of tools included in FSL along with brief descriptions on the

subprograms can be seen in appendices: appendix 10 for all the included MRI tools and appendix 11 for other tools.

6. SOFTWARE IMPLEMENTATION METHODS

The white matter neural tract analysis in this research was conducted on a 32-bit Windows environment PC with 3 GHz Intel Pentium 3 Xeon processor and 4 Gb of RAM. Voxelwise statistical analysis was conducted using three different software suites; MRIConvert [26] for image format conversions, VMware Player [30] for emulating Linux environment in a Windows environment, and finally FMRIB Software Library version 4.1.9 [1] for the whole analysis process including preprocessing and artifact reductions. The analysis of the FA data was carried out using TBSS [3], which is a part of FSL. After altering the diffusion images to the correct form, various preprocessing steps were taken to ensure that the quality of the images was sufficient for the analysis process. FA images were then created by fitting a tensor model to the raw diffusion data using an FSL subprogram FDT/DTIFIT, and then brain-extracted using BET [27]. Subjects' FA data were then aligned into a common space using both affine alignment and the nonlinear registration tool FNIRT [31] [32] (implemented within the TBSS scripts), which uses a b-spline representation of the registration warp field [33]. Next, the mean FA image was created and thinned to create a mean FA skeleton which represents the centers of all tracts common to the group. Each subject's aligned FA data was then projected onto this skeleton and the resulting data fed into voxelwise cross-subject statistics.

6.1 Image data

Image data for the implementation process was provided by Tampere University Hospital. The data included a control group consisting of 40 individual MR diffusion image sets and a group of 35 patient diffusion image sets; a total of 75 brain diffusion images. The control group consists of healthy individuals and patient group includes individuals with different levels of spinal cord injuries. In order to properly test the functionality of the software, the two groups are required to be different in terms of white matter FA, thus a group of patients with assumed structural differences in neural tracts was used. The image data was taken with 20 different diffusion gradient directions a $b = 0$ weighted image, each taken three times. Due to hardware and software restrictions, a total of 48 images were used in the process, 24 control images and 24 patient images. These two groups formed the patient and control groups used in the TBSS analysis, and details of these two groups are presented in table 6.1.

Table 6.1: Details of the two groups of subjects used in TBSS analysis. Age is presented as average ± SD.

Group	Count	Age	Females	Males
Control	24	43.21 ± 10.98	11 (45.8%)	13 (54.2%)
Patient	24	52.21 ± 13.56	4 (16.7%)	20 (83.3%)

Being in a wrong format for FSL to read, the image data was first converted into NIfTI format, and MRIConvert was deemed valid for this purpose. The conversion was executed so that the images were converted to FSL NIfTI -format, which differs from the generic NIfTI only by slight changes in header information which allow FSL to process the files easier, but is still fully compatible with the NIfTI format. Patient ID was selected for naming the files in order to be able to identify the data and separate it into different categories. Files were saved as .nii files, each in the same directory as a 4D file. The software can convert multiple images simultaneously, and the whole diffusion data set was converted at one execution. See figure 5.3 for an overview of the user interface of MRIConvert.

6.2 Preprocessing

After converting the whole image data to the appropriate format, it is then ready to be preprocessed. First a program for eddy current and patient head movement caused distortions correction was run; Eddy Current Correction (see chapter 5.2.2 for details). Both corrections are done by same program, requiring only the reference volume (the image volume with no diffusion weighting, which is usually volume number 0 as was in this case) as input in addition to the filenames of the input 4D image being corrected and the output. In order to process the whole set of image data consequently, a custom script that feeds the program all the images was created. The resulting error corrected images were saved in a different folder in order not to confuse them with the original data.

For TBSS scripts, a binary brain mask for each image file is required to rule out all but brain tissue from the images. The brain masks are created by a program called Brain Extraction Tool. Details of its use can be found in chapter 5.2.3. Because only the binary brain masks were required, not the default brain image output, the following options were used: `-n -m -f 0.3`. The fractional intensity threshold of 0.3 was experimentally defined to be the most practical value for our image set. All the images were processed consequently via a custom Linux script. The brain masks were saved in their own folder in order to ease the segregation of different file types.

Next stage was the creation of FA images by fitting a tensor model to the corrected diffusion data by DTIFIT. Because DTIFIT can only process one diffusion image

at a time, a custom script to consequently process the images was used. DTIFIT requires the original b-values and b-vectors files associated with the corresponding NIfTI image files as inputs. The created brain masks are also used in this phase to rule out non brain tissues. Because this phase has ten outputs per image, it is important to define a new output directory where the fitted images will be saved. No optional parameters were used for the tensor fitting procedure. The created FA images were next moved to a new folder in which the TBSS phases would take place.

The first TBSS script. `tbss_1_preproc` is actually a part of preprocessing. It is run in the folder where all the FA images were moved, and it basically only erodes the FA images and moves them to a new folder. As a result of this phase a simple html layout is created in the folder `./FA/slicesdir` which should be used to review the images for rough errors. The script only requires the FA images as input, and can simultaneously process all the images by using the asterisk sign as input, as described in chapter 5.2.5.

6.3 Image registration

Image registration can be done in a couple of different ways in TBSS, either by using a pre-defined target or by telling the program to automatically search for the most typical subject to use as a target image. The included standard space image FMRIB58_FA was used in all the registration processes as a target.

The registration step is easy to perform, but quite time consuming. It was run with the command `tbss_2_reg -T`, where `-T` indicates that we want to use the FMRIB58_FA as a target. The script automaticallly goes through the whole data when called, and the only input needed is the choice of registration target. According to the FSL website, the registration phases are divided between this script and the next one, but as the next phase already constructs the FA skeleton, it is divided into its own section. After this phase and the registrations are done, no visible results are available, but the next phase can be started as soon as the script is finished.

6.4 Skeletonization

This phase concentrates on finishing the registrations and creating FA skeletons. Standard space versions of the FA images and a mean FA image are created first, then the mean FA skeleton is derived. This was done by the command `tbss_3_postreg -S`, where the `-S` indicates that we wanted to derive the FA skeleton from our image data rather than use a ready skeleton map.

When the script finished, the mean skeleton was viewed with FSLView, and a threshold of 0.3 was deemed suitable for the data used in the analysis. This threshold was then input to the next script, which removes parts of the skeleton

under the defined FA value and projects all the subjects' FA data to it, creating a 4D file with skeletonised data. This was done by running `tbss_4_prestats 0.3`. When the script finished, the data was ready for groupwise analysis.

6.5 Statistical group comparisons

Now the file `all_FA_skeletonised`, containing a skeletonised FA image of each subject was fed into the Randomise tool. The tool can be used for several purposes, but we used it for a two sample t-test which would determine areas of the skeleton which have statistically significant differences between the two given groups. The files were named so that the control group was first in an alphabetical order. The script `design_ttest2 design 24 24` was used to easily create the design matrix and contrasts file for a simple two group unpaired t-test. The script needs to be run in the `stats` folder, and the numbers input describe the group sizes, which for our case was 24 controls and 24 patients.

With the design files and skeletonised data ready, the following command was then run in the `stats` folder:

```
randomise -i all_FA_skeletonised -o tbss -m mean_FA_skeleton_mask
-d design.mat -t design.com -n 10000 -T2.
```

This script uses the FA skeleton data, the thresholded mask (with FA value 0.3) and the created design files, and output the resulting files of a statistical group comparison with prefix `tbss`. The null-hypothesis is generated via a set of ten thousand permutations and the TFCE method is used for defining which voxels are statistically different between the groups. When the permutations are done, the results are saved as images in the same folder where the script was run and can now be visually inspected.

6.6 Cluster information

Detailed information on the significant clusters were derived from the randomise output images. Cluster sizes, cluster p-values, cluster mean FA values and cluster minimum p-value locations were derived from the data. The following command was used to obtain sizes of clusters, cluster sizes, positions of minimum p-values

```
cluster -in=tbss_tfce_corrp_tstat1.nii.gz -thresh=0.99
-oindex=clusterindex -olmax=clustermax.txt
 osize=clustersize > clustertable.txt
```

The script outputs two text files and two mask images. The text files include cluster local maximum locations and values (`clustermax.txt`) and information on cluster

index, size, 1-p value, maximum 1-p value locations and 1-p value center of gravities for clusters (`clustertable.txt`). The image files generated by this command include cluster mask images with clusters specified by size (`clustersize.nii.gz`) or by their index number (`clusterindex.nii.gz`). The image with cluster index classification is easier to work with and it was used to handle the clusters.

To obtain mean FA values of the clusters for patient and control groups, the cluster mask image using indexes was divided into mask files corresponding each cluster:

```
fslmaths clusterindex.nii.gz -thr 1 -uthr 1 -bin clustermask_1
```

This command was repeated for each cluster number, changing the corresponding thresholds and output names. The threshold needs to be the same to create a mask with only one cluster. Now a file with data on average FA value on the clusters for each patient and control image was created with command:

```
fslmeants -i all_FA_skeletonised.nii.gz -o voxeldata_cluster1.txt
-m clustermask_1.nii.gz
```

The command was repeated for each cluster with corresponding cluster mask file and output filename. The received data was then processed with Excel to obtain average FA values of the cluster for patient and control groups as well as the mean FA difference for the two groups.

7. RESULTS

In this chapter the concrete results of the analysis process will be presented along with some data on the performance of the software. The analysis is split in different stages in a similar manner as in chapter 6. One section will concentrate on the usability and overall functionality of TBSS. Any problems or inconveniences experienced during the analysis process will also be addressed.

7.1 TBSS analysis results

Results of each of the different stages will be presented shortly, with the final results of the analysis in the last subsection.

7.1.1 Preprocessing

Eddy current correction corrects for head movement during the scan and for geometrical aberrations caused by gradient fields. There was hardly any head movement nor clearly visible eddy current artifacts in the data series used in the implementation, thus any visible results for this operation would be hard to present. The next operation in preprocessing stage is the creation of a binary brain mask, which is followed by the creation of different diffusion images by fitting the tensor model to the diffusion data. An example of a diffusion MR image along with its brain mask and resulting FA map is shown in figure 7.1. The original image is only a presentation of one of the diffusion gradient directions, whereas the FA map is constructed using all the directional gradient information.

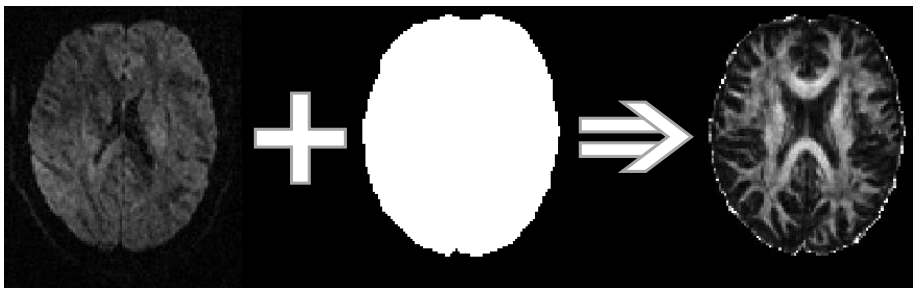

Figure 7.1: Results of the preprocessing stage summarized in one figure. An example of a pure diffusion image from one magnetic diffusion gradient direction on the left, its binary brain mask in the middle and derived FA map on the right. The resulting FA map on is achieved with the diffusion image, brain mask and tensor data.

7.1.2 Image registration

In the registration stage of TBSS, all of the FA maps are registered to a standard space resolution and to a common target provided by FSL. In figure 7.2 the same target as in figure 7.1 is used to demonstrate the effect of registration to the standard space FMRIB58_FA image.

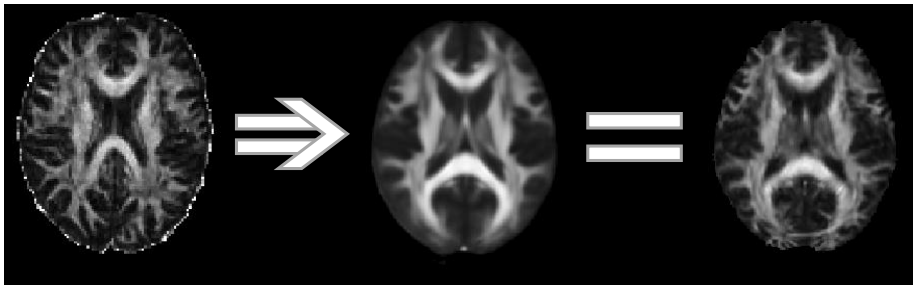

Figure 7.2: Image registration process. The FA map shown on left is registered to the standard space image in the middle via affine and non-linear registrations. The shown result (on the right) is achieved by running the registration TBSS scripts.

7.1.3 Skeletonisation

After the images have been aligned and non-linearly registered, the FA skeletons are derived. First the mean FA image is created as an average of all the subjects used in the analysis, then the mean FA skeleton is derived from the mean FA map. The FA skeleton is usually shown on top of the greyscale FA image with green coloring. The mean FA map and mean FA skeleton is shown in figure 7.3. After the creation of the skeleton, it is cropped with a FA value of 0.3.

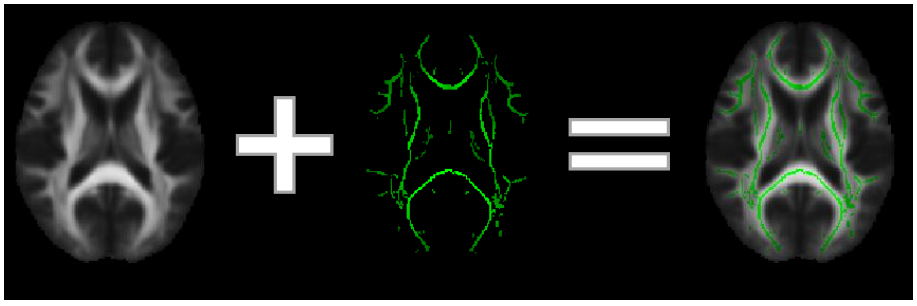

Figure 7.3: Product of skeletonization process. Mean FA map on the left, its skeleton in the middle and the skeleton overlaid on top of the mean FA map on the right.

7.1.4 Statistical group comparison

In the last stage of the actual TBSS procedure all the FA skeletons are fed to the randomise program, which calculates voxelwise statistics for the differences between

skeletons in user defined groups. The results are in visual form as $1 - p$ values. In figure 7.4 the resulting image with statistically significant areas of the skeleton is presented. The image is also overlaid to the mean FA and skeleton in a manner often used for representing the final results.

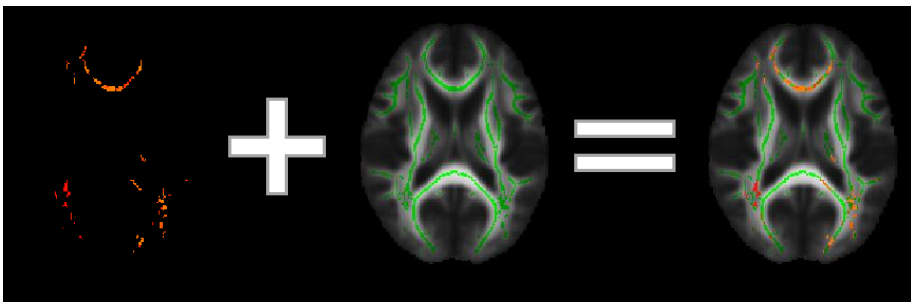

Figure 7.4: Statistically significant areas are shown on the left, with mean skeleton and FA map in the middle. The resulting image on the right serves as an illustration of how the results are usually viewed. Color scale and values are exactly same as in figure 7.5, but are not included in any of the interphase result images for simplicity.

7.1.5 Statistically significant clusters

The results with significant differences in FA maps between the two groups used in the analysis can be seen in figure 7.5. Mean FA map is presented in the background in greyscale with the mean skeleton in green. On top of the skeleton are the areas (or clusters) of significant differences between the patient and control group, and in this particular case the significant areas represent clusters where patient group mean FA value is significantly decreased compared to control group mean FA values.

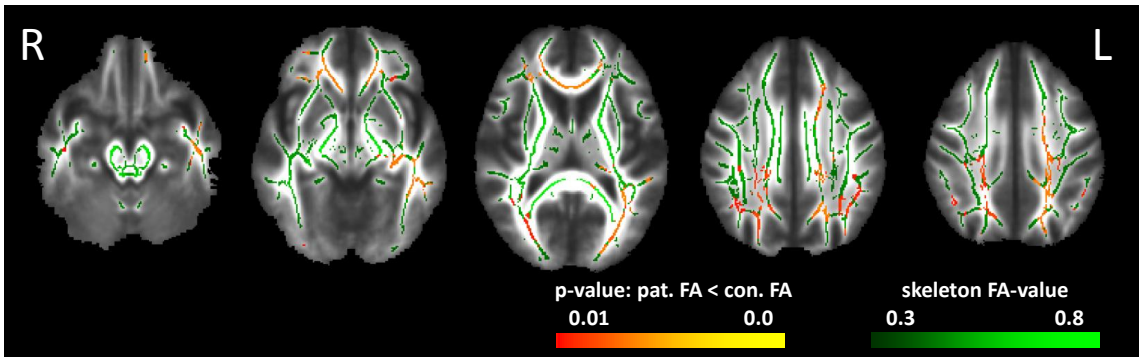

Figure 7.5: Five sample images of the qualitative results from TBSS analysis for the used patient and control database. Significant differences, where patient FA is lower than control FA, are visualized with red-yellow coloring, according to corresponding the p-value of the statistical difference. Mean FA skeleton is presented in green color under the significant clusters.

Cluster information was extracted from the images, and five different clusters were found with the p-value less than 0.01. The significant clusters are presented

Table 7.1: Significant clusters tabled with their sizes, maximum values of $1 - p$ and their locations in voxel coordinates (millimeter coordinates can also be used). Note the huge cluster size of cluster no. 5. The clusters are visualized in figure 7.6.

Cluster index	**Voxels**	**Max.** $1 - p$	**Max. X**	**Max. Y**	**Max. Z**
5	12244	0.996	90	150	85
4	4590	0.993	61	68	92
3	406	0.992	117	165	71
2	213	0.99	47	109	55
1	16	0.99	116	144	71

Table 7.2: Local maxima of cluster number 5 ($1 - p$ values) and their locations in voxel coordinates. Locations of the maximas are visualized in figure 7.6.

Maximum no.	$1 - p$	**X, voxels**	**Y, voxels**	**Z, voxels**
1	0.995	105	74	122
2	0.995	107	73	120
3	0.995	111	73	114
4	0.995	106	83	112
5	0.995	108	82	112
6	0.995	110	78	112

in table 7.1. The two largest clusters are really large which indicate extensive areas with significant differences. Local maxima of the clusters were printed out also, but for convenience only the local maxima of the largest cluster are shown in table 7.2. The five clusters of significant differences and local maxima of cluster five are both also shown in figure 7.6 for a more elucidative presentation.

The cluster information output also includes mean FA values of each significant cluster for each analyzed image; patient and control. Once again for the sake of convenience, all the mean FA values are not reported, but the mean values for patient and control groups for each significant cluster are listed in table 7.3 along with the difference between the mean FA.

Table 7.3: Mean FA values of the significant clusters with standard deviations. The difference is calculated by deducting patient FA from control FA values.

Cluster	**Mean FA, control**	**Mean FA, patient**	**Difference**
1	0.5599 ± 0.0687	0.4806 ± 0.0636	0.079204 ± 0.0936
2	0.5202 ± 0.0376	0.4615 ± 0.0479	0.058677 ± 0.0609
3	0.4256 ± 0.0304	0.3722 ± 0.0394	0.053377 ± 0.0498
4	0.5259 ± 0.0257	0.4775 ± 0.0391	0.048416 ± 0.0467
5	0.5261 ± 0.0274	0.4791 ± 0.0407	0.046974 ± 0.0490

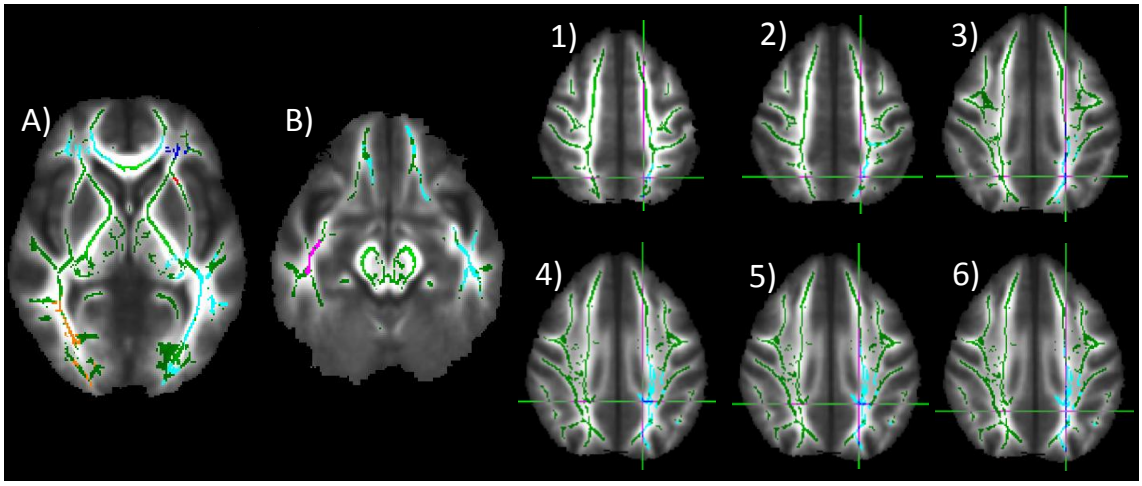

Figure 7.6: Five most significant clusters in the results are presented on the left (A and B) with the following coloring: 5=cyan, 4=orange, 3=blue, 2=magenta and 1=red. The six local maxima of cluster five are presented on the right with corresponding numbering to table 7.2.

7.2 Analysis efficiency

Because the GUI versions of most tools only process one image at a time, the terminal command utility was applied by utilizing a script which goes through all the image data, processing several images consecutively without user input. The script runs through all the different phases of the analysis process enabling the user to run the whole TBSS analysis with only one command. Even with the application of such a script, the whole analysis process is quite time-consuming.

Time taken by the whole process is almost linearly related to the amount of data; the process which takes most time is the eddy current correction, which is done to each image. Time taken by different stages of the analysis is reported in table 7.4. The time information was taken by running the original analysis of 24 patients and 24 controls over again with added commands in the script, which save the run time of each individual step to text files. Run times of eddy correction, BET and DTIFIT are rough averages of one image process time multiplied with the amount of images processed and can thus include some amount of error. Timestamps were also recorded when the script was started and when the script had finished; start time was Tuesday 13.50,02 and end time Thursday 14.50,34. Total time via timestamp evaluation would thus be 49.009 hours. Run time of image conversion process is not included in the efficiency evaluation.

Performance was also evaluated with the evaluation data suite included in the software. The FSL website includes a reference table with speed evaluation results of various different configurations; this data is presented in table 7.5 along with the result obtained by running the evaluation for the used PC configuration. The speed

Table 7.4: Run times of different stages of the whole TBSS analysis.

Phase	Derivation method	Run time (h)	Percentage (%)
eddy_correct	33min×48	26.40	54.49
BET	4sec×48	0.0533	0.11
DTIFIT	20sec×48	0.2667	0.55
tbss_1	Exact run time	0.1239	0.26
tbss_2	Exact run time	4.1325	8.53
tbss_3	Exact run time	0.5422	1.12
tbss_4	Exact run time	0.3825	0.79
randomise	Exact run time	16.551	34.16
Total sum	Sum of phases	48.452	100

comparisons are made with the test script mentioned in section 7.3 by using a timer command which clocks the run time of the evaluation script.

7.3 Functionality of TBSS

There is an evaluation and example data suite available for download, which can be used for two purposes; either for testing the proper functionality of all the tools included in FSL or for running FSL with example data included in the package. For evaluating the tools there is a script `RUN`, which can be used to execute all the tools included in FSL and compares the results with output data included in the data suite. Running the evaluation is a good way to make sure everything is working as intended in FSL. The example data can be used to familiarize oneself with some of the tools.

Although TBSS is a multi-subject comparison tool, some of the programs used in the analysis process do not natively support processing of multiple targets simultaneously or consecutively without user input between subjects; eddy correction, BET and DTIFIT each can only process one image at a time. Although these tools are not directly related to TBSS analysis, but to the preprocessing stage, they are compulsory phases in order to obtain the best results possible. Apart from the minor inconvenience with multiple image consecutive processing, there were no significant problems with the TBSS analysis.

Table 7.5: FSL evaluation and example data suite timings for different hardware setups for version 4.1.0-5. Courtesy of University of Oxford. [34] Test result with the used configuration is highlighted.

Hardware	**OS**	**Time (s)**	**Relative speed**
Intel Core i7-2600K 16GB	Ubuntu	954	0.52
Apple MacBook Pro 17' laptop 2.3GHz Intel Core i7 8GB	OS X 10.6.7	1093	0.61
Dell Precision T7500 Xeon W5590 3.33GHz 64 Bit 12GB	Ubuntu	1201	0.67
Apple MacBook Pro 17' laptop 2.66GHz Intel Core i7 8GB	OS X 10.6.3	1430	0.79
3GHz Intel Pentium 3 Xeon 4GB, Win XP & VMware	**CentOS 5**	**1604**	**0.89**
Apple MacBook Pro 17' laptop 2.93GHz core 2 duo 64bit 8GB	OS X 10.5.6	1638	0.91
Dell PowerEdge 2950 Server 2xQuadCore 3.16GHz Xeon 32GB	RH EL 5	1675	0.93
Apple MacBook Pro 15' laptop 2.8GHz core 2 duo 64bit 4GB	OS X 10.5.5	1694	0.94
Apple MacBook Pro 17' laptop 2.6GHz core 2 duo 64bit 4GB	OS X 10.5.4	1801	1
Apple Mac Pro 2.8GHz 8-core 64bit 8GB	OS X 10.5.4	1823	1.01
Dell Optiplex 960 3.4GHz 2-core 4GB	Ubuntu	2115	1.17

8. DISCUSSION

The version of FSL used in the implementation is 4.1.9, but during the writing process a new version of FSL was released. On September 2012, version 5.0 was released along with an entirely renewed Wiki-based website. Some of the tools were also renewed, but no significant changes were supposedly made to the TBSS analysis. Some minor improvements were made to the documentation along with minor adjustments to the performance and accuracy of some tools.

8.1 MRIConvert

The choice of software for image type conversion could have been made differently, the current software had some problems with the folder and file structures of the DICOM images; it did not function with long file and folder names. The problem can be avoided by using simple filenames and a minimal amount of tersely named subfolders. Exporting images from an archive may automatically lead to long file names and they need to be renamed before MRIConvert can process them.

Some of the options in MRIConvert need to be enabled for correct output file types. These options include saving multi-volume series as 4D files and saving the files as .nii -files. The older .hdr file extension should also be compatible with FSL, but the newer .nii is recommended. As for multi-volume series saving, the 4D files are compulsory for the data to be processed correctly. Using a different software for the whole conversion process is also an option; the choice of software should not have an impact on the results.

8.2 Significant clusters

Accuracy of the method and biases related to it are discussed further in section 8.5. Accuracy of the statistical differences indicated by the randomise program is greatly affected by the chosen method. Amount of randomizations have an effect on the accuracy as well, but the error is sufficiently small when using at least 5000 permutations; lower amounts would decrease accuracy significantly, but adding to the number of permutations does not have such a substantial effect. The FSL website recommends 10 000 permutations if time permits.

The chosen thresholding method has the most effect on the significance of the results. Voxel based thresholding is the least accurate since it completely disregards

neighboring voxels in the analysis. Even small, only one pixel sized differences will be registered, which greatly increases the probability of an image bias (noise, artifact) being interpreted as anatomical structural difference. Cluster based thresholding, either size or mass, give slightly better and more accurate results, but the problem with both thresholding methods is that they require a user set minimum threshold value for the mass or size of the clusters. Finding a suitable cluster size can take some time and produce unnecessary analyses with either excessively large or small cluster thresholding.

Threshold-Free Cluster Enhancement is a new method for cluster thresholding proposed by Smith and Nichols [29] in an FMRIB Technical report. The method is recommended to be used with TBSS, and it is the method that was used in this thesis. Using TFCE overcomes at least two problems that are encountered using other methods; the need for choosing a cluster size or mass value for clusterwise thresholding and the inaccuracy of voxelwise thresholding. The TFCE method is neither voxel based nor cluster based method, although it does work similarly to cluster based methods. Instead of only searching for certain sized clusters or single voxels for differences, TFCE enhances areas of with spatial continuity. Clusters are intensified and noise is effectively ruled out of the results. Voxel based methods usually require a p-value of 0.001 or less for the results to be considered significant. Such small p-value also increases the risk of a type II error compared to, i.e., a probability threshold of $p < 0.05$. In addition to this, voxelwise statistics ignore any neighboring voxels, which often causes biases with imaging data. [35]

The areas with significant differences between the control and patient groups are shown in figure 7.5, in which the different clusters are not specified. In this analysis the effect of age on white matter and axon structures can be clearly seen from the large area of differences. Age has a major effect on brain connectivity, which has a direct impact on neural tract structures and is thus seen as a drop in FA values. The patient group has a notably higher mean age (see table 6.1) which explains the drop in FA in such a widespread area. The results are in this sense biased, and the effect of the spinal cord injury in the patient group is hidden under age related effects.

8.2.1 Cluster sizes and maxima

Table 7.1 holds information on all the five significant clusters: cluster sizes in voxels, maximum significance level and its location in voxels. The size of cluster 5 is notably large due to the vast amount of neighboring significant voxels found in the analysis. The size of the clusters can be reduced by lowering the threshold value of p. The location information can be also output in the MNI standard space coordinates. From image 7.6 we can see that the cluster number 5 is really extensive and reaches both hemispheres of the brain.

Looking at the local maxima of cluster 5 in table 7.2 we notice that the local maxima locations differ from the maximum location reported for cluster 5 in table 7.1. This is due to the large volume of the cluster; there are dozens of maximum values in the cluster, and if they would all be printed out the global maximum would be included amongst the local maxima locations. The global maximum $1-p$ value for cluster 5 is 0.996 but local maxima values are reported as 0.995 instead. This could be an error in rounding, because the location of global maximum is still included in local maxima locations. No errors were given by the analysis, and the results do seem somewhat confusing. No information referring to a similar type of bias in the results were found from the support forums.

All the local maxima of cluster 5 seem to be close to each other, which indicates that the most significant cluster would reside around the area of these maxima if the threshold would have been chosen lower. The maximum locations, i.e. the locations of most significant differences, from the analysis are a good indicator for areas where changes in axon structures should most probably occur. These areas can be used as references for seed points in ROI based analyses.

8.2.2 Fractional anisotropy values

The mean FA values in table 7.3 are calculated by deriving the average FA value of each cluster from each of the input images (patients and controls), these averaged values are again averaged between the control and patient groups. The biggest and most significant cluster, 5, also has the largest difference in FA values between the control and patient groups. As the significance level drops, the FA value difference also reduces. For some of the clusters the difference is smaller than standard deviation, but for example the vast size of cluster 5 partly explains the dispersion.

Cluster 3 has noticeably lower FA value when compared to the other clusters. This can be explained by looking at its location from figure 7.6; the cluster is located at the peripheral area of the FA skeleton. What this means is that the area inside the cluster contains less neural tracts in general than the other clusters. The peripheral areas also have more subject-wise variation than the core parts of the skeleton. With fewer axons in the area, diffusion has less restrictions and is more isotropic, leading to lower FA values. Also intersubject deviations in the peripheral areas can cause a bias to the calculated mean FA, which appears lower than it should.

8.3 Performance

The version of FSL used in this thesis (Release 4.1.9) supports 32-bit architecture in addition to 64-bit, which is a bit of a trade-off; the software can be run on older platforms and hardware, but on the other hand 32-bit architecture has its limitations

in handling large data quantities. For medical image analysis the memory limitations of 32-bit hardware can be severe, and with 64-bit hardware and software there are no real limitations to the size of the analyzed data. With the FA image data used in this research, only 48 images could be processed with TBSS, and for ADC analysis the amount is even lower.

The performance results reported in 7.5 suggest that the configuration used in the analysis is more than capable of running the analysis software in a decent time. The fastest hardware in the table runs the analysis in almost half the time compared to the setup used in this thesis, but it should be noted that the fastest hardware setup is really high-end.

The performance, or the run time measurements, of TBSS analysis were reported in table 7.4. Although these values cannot be directly compared with time evaluation results in table 7.5, they are a good indicator of performance of the TBSS analysis itself. Clearly the most time consuming phase is the preprocessing and eddy current correction. Even the nonlinear and linear registrations done in the TBSS script phase take much less time. The second most time consuming phase is the randomise script, which compares the two groups and finds the significance levels of differences by a statistical t-test. A total of 97.18% of the whole run time is taken by eddy current correction, TBSS registration and statistical testing phases. For multiple analyses with the same image data, the preprocessing phases (eddy current, BET and DTIFIT) are required to run only once, reducing the time of subsequent analyses with the same image data.

8.4 Usability

The usage of FSL is made effortless by good instructions found on the software's website. The downside is that the ease of use seems to be mostly restricted to the basic functions of FSL, for example in TBSS analysis only the basic portion of the analysis process is covered. Further information and valuable tips can be found at the FSL forum website. The forums are an excellent source of information if one has trouble with some of the program features or wishes to extract advanced information on the results. The basic output given by following the website's instructions can in some situations be insufficient. This was the case also with TBSS analysis; running the analysis by following the instructions gives results only as a figure, and no numerical values are presented. Browsing the FSL forums for a while taught that numerical values can be derived with relative ease from the visual results. On the other hand the instructions cannot cover every small detail in the whole software library, but it should be mentioned that there are advanced features available. At this state the user basically has no clue if there is a way to i.e. derive numerical results from TBSS analysis results.

Another downside is processing multiple subjects with some of the tools. There is no evident way to i.e. preprocess images; the subprograms can only process one image file at a time. This problem can be bypassed with the use of Unix shell scripts, but for everyone this may not be self-evident. Using self-made scripts also means that one has to use the command line utilities instead of the easier GUI.

Even though there are downsides in the software from usability's point of view, there is also a lot of good in the software when it comes to usability. First of all, the fact that the software actually has a graphical user interface in the first place is nice. When you add the tooltip help texts to the GUI that pop up when you hold the cursor on any of the fields in a tool, the user experience gets really smooth. For example, processing a DTI image by correcting it eddy currents and structural deformation, removing non-brain tissue, creating its FA and ADC maps and for example running probabilistic tractography on the subject can all be done via the GUI.

Command line utilities for the subprograms are sufficiently simple to use also. Each program includes a help command which prints out the available options and how to run the command. If one has even mediocre experience with Unix shell commands, the FSL command line utility usage should be effortless.

Installation of the software is also made easy, and at its easiest the installation only requires execution of one script which will download, install and configure the FSL environment in a Linux based (CentOS is the recommended Linux version for running FSL) computer. For Windows environment the installation is almost as easy, and only addition to the installation process is setting up the virtual Linux environment with VMware Player.

8.5 Criticism of the methods

A lot of criticism towards TBSS and diffusion image analysis in general has been stated. Some of the points presented by Jones and Cercignani in their article *Twenty-five pitfalls in the analysis of diffusion MRI data* [36] will be reviewed in this section. The main idea behind the critique towards diffusion imaging is the low imaging resolution currently available with tolerable scan times and errors due to different stages of the analysis process.

8.5.1 Criticism of diffusion imaging

The main source of flaws and biases in the acquired diffusion images is obviously the image acquisition process. With the current MRI equipment the quality of the diffusion data is considerably improved, but even still the scan times would be too long for obtaining sufficiently accurate images. The largest source of uncertainty

and error is the acquisition stage, but also each step in the image analysis brings its own possible source of error to the results. Thus the overall uncertainty in the inference of the analysis is the cumulative error from each individual stage of the whole analysis process.

Many of the problems stated by Jones and Cercignani [36] are also related to the acquisition stage. The most important thing that they state is that the diffusion data used in the analysis should be scanned with exactly the same parameters. Several imaging factors affect the analysis results: the used b-values, used acquisition angles, acquisition resolution and pretty much all the factors affecting the diffusion images. The best results in a group analysis will be achieved by comparing images taken with the same scanner with the exact same imaging parameters.

Eddy current correction is one of the processes which are susceptible to flaws. Most eddy current correcting algorithms use global affine registration to correct the distortion, which means that the whole brain data is registered for example to the $b = 0$ image, and only a single affine transformation is used for each slice. This neglects the fact that eddy currents vary slice by slice, and the correction results can be only moderate. Correcting slice by slice is much more calculation intense and probably thus less common in analysis software suites. Another problem arising from eddy current corrections is connected with the signal intensity within a voxel. Eddy current correction changes the voxel shape and thus probably changes the information content of the voxel. The signal intensity of the voxel will be changed with an inverse relation to the change in the size of the voxel, and if the signal intensity is not modulated according to the volumetric change, the voxel signal information will be biased. [36]

Motion correction is a vital part of the preprocessing stages, particularly if the image acquisition times are longer. Involuntary patient motion during scans is basically unavoidable, and needs to be taken care of by image processing. Although motion correction by affine image registration is very elementary and effective procedure to correct patient motion, one aspect is often left unnoticed; the diffusion encoding gradients. Each diffusion image is related to its corresponding diffusion gradient, and when rotating the images and leaving gradient directions untouched, the overall diffusion information will be biased. The effects of neglecting the diffusion gradient directions can produce erroneous diffusion directions, i.e. FA vectors will point in the wrong direction. Fortunately the TBSS method is unaffected by the directional information of diffusion, as well as FA direction; only the absolute scalar value of FA is relevant. The effects of biased gradient information would be seen for example in the color coded FA maps. [36]

When fitting the tensor data to the image data, the most often used method is linear least squares fitting. Fitting the tensor data linearly includes the assumption

that noise in the data is independent and identically distributed. This is definitely not the situation in reality. In reality any kind of noise in the acquired image is usually not evenly distributed, nor most artifacts. Using non-linear fitting may reduce the effect, but will not remove the error. Also comparing images with different methods of tensor fitting will most likely lead to biased results. [36]

Some of the other mentioned pitfalls are issues with small FA values and noise, different solutions in voxel based methods for linear and nonlinear normalization and amount of warping in registrations. These errors concern voxel based methods in general, but TBSS with its skeletonization bypasses these problems quite efficiently. Because quite many of the issues do not concern TBSS, they are ignored and TBSS related pitfalls are addressed in section 8.5.2.

8.5.2 Criticism of TBSS

Most pitfalls related to TBSS concern the skeletonization method; although it overcomes many earlier issues with i.e. registration, no method is perfect and also the act of skeletonization brings forth new issues. The first issue is the impact of macroscopic lesions on the skeletonization stage. Jones and Cercignani [36, pp. 818–819] suggest that a white matter abnormality (MS lesion, tumor or stroke originated), which would likely reduce local FA values, would likely have an unpredictable effect on the skeletonized FA image. It is true that the FA values will be likely reduced in the area of these lesions, or the FA values for the tract voxel will be read from a wrong location. In both cases however, the result will be that the FA values are abnormal, thus suggesting a neurological condition, which is, all due respect, the basic purpose of the analysis. If a tumor exists in the white matter area of the current subject, it is most likely been noted before the diffusion image analysis, and will not affect the inference. In the case of MS lesions the claim of a pitfall is absurd; the point of TBSS analysis is to find the areas with these lesions (significantly different FA values), how can the effect of MS lesions to the skeleton FA values be a pitfall? For stroke originated changes in white matter the case is similar; DTI can be used to evaluate stroke effects and thus the effect of stroke to skeleton FA values seems only a favorable matter when it comes to detecting and evaluating effects of a stroke [37].

Another matter which was addressed by Jones and Cercignani [36, pp. 818–819] is the skeletonization process itself, and the co-registration of image data in order to achieve correct skeletonization. They point out that no error is given if the registration in the TBSS tools would for some reason fail or give biased results. The process is largely automated, and there is not much intermediate output from the programs. It is recommended to check the skeletonization and its alignment to all of the FA maps. If this is not done, the skeletonization and co-registration could include errors that would give biased analysis results.

Crossing fibers is a problem that is associated with all voxel based methods, but perhaps even more with TBSS and skeletonization. Each voxel contains dozens (hundreds, depending on the acquisition resolution) of tracts and if the fibers cross inside a voxel the FA is interpreted falsely; the FA value of such voxels are often lower than they should be, and the directional information can be erroneous. Crossing fibers can lead to wrong FA values in the FA skeleton and thus ultimately to wrong inference. There are some probabilistic methods which are supposed to fix some of the problems caused by crossing fibers, but they are out of scope of this thesis.

8.6 Clinical point of view

Numerous amounts of articles which address TBSS analyses on neurological conditions have been published. These analyses include conditions such as dyslexia [38], systemic lupus erythematosus [39], autism spectrum disorder [19], bipolar disorder [40] and various other neurological conditions. The results in the publications seem always positive by nature, and for each type of condition a certain change in white matter structures are found. TBSS has its flaws, and even if the published analyses were unanimous, one should still sustain a level of skepticism towards the results.

Although the results can be characterized as clinical results, and in some cases the results can indeed reflect the effect of a disorder to the neural tract structure of a single patient, one cannot neglect the fact that the analysis is designed only for multi-subject studies. In this light the software can mainly be used in research purposes, for it is impossible to apply the analysis for a single patient. For neurological conditions with identical or similar patient-wise effects on white matter structure, the method is very capable in finding out the common effect. TBSS can be applied to different neurological conditions in research use. The analysis results can also be used as a supporting method in ROI based measurements, or as a map of areas which should contain the largest divergences in measured quantities.

At its current stage of diffusion imaging technology and TBSS analysis software, the results include many sources of error and the analytical use should be restricted to a supporting role. The TBSS analysis definitely has its uses, but mainly as a supporting software for other type of diffusion data analyses.

9. CONCLUSIONS

Diffusion MR imaging is an interesting branch of magnetic resonance imaging, and it can be used to derive microscopic structural elements otherwise invisible to other imaging modalities. Brain white matter and neural tract structure is the most studied subject with diffusion MRI. A relatively new MR diffusion image analysis software was implemented for the use of Tampere University Hospital along with this thesis. The analysis process is described in detail in this thesis, and the purpose of chapter 5 is to present the whole analysis process as well as serve instructions for the procedure.

Spinal injury patient data was compared in a groupwise analysis against a group of healthy volunteers. Diffusion image data was processed with different tools included in FMRIB Software Library and the multi-subject white matter analysis was performed using Tract-Based Spatial Statistics. The analysis results of TBSS consist of areas with statistically significant areas of certain quantity (FA, ADC, diffusion tensor eigenvalues) presented visually. The analysis covers the whole white matter area and compares major neural tract bundles between various user defined groups of subjects. Quantitative results on the statistically significant clusters can be derived in addition to the visual results.

Results of the analysis ran in this thesis indicates at least two things: the analysis is functional, but also the effect of age on neural tracts is so severe that ignoring it will lead into biased results. The results show mostly the effect of age on white matter; the areas of white matter with lowered FA values reside mostly in areas which should be most affected by aging. Also the large areas of significant differences point out that it is not only the spinal injury which is causing the FA values differences. Further analyses should always be age matched in order to obtain acceptable results. In order to obtain correct analysis results for the groups used in this thesis, the groups need to be modified in order to make them more age matched and the analysis needs to be rerun. In general the analysis is a good supporting method for different type of neural tract analysis methods. One should take caution when drawing inferences based on only TBSS analysis results.

REFERENCES

[1] Smith SM, Jenkinson M, Woolrich MW, Beckmann CF, Behrens TEJ, Johansen-berg H, et al. Advances in functional and structural mr image analysis and implementation as fsl. NeuroImage. 2004;23:208–219.

[2] Woolrich MW, Jbabdi S, Patenaude B, Chappell M, Makni S, Behrens T, et al. Bayesian analysis of neuroimaging data in FSL. NeuroImage. 2009 2009 Mar;45:S173–86.

[3] Smith MS, Jenkinson M, Johansen-Berg H, Rueckert D, Nichols TE, Mackay CE, et al. Tract-Based Spatial Statistics: Voxelwise Analysis of Multi-Subject Diffusion Data. FMRIB Technical Report TR05SS1 (a related paper has been accepted for publication in NeuroImage). 2005;p. 26. Available from: `http://www.fmrib.ox.ac.uk/analysis/research/tbss/tr05ss1.pdf`.

[4] Myers HP. Introductory Solid State Physics, Second Edition. Taylor & Francis; 1997.

[5] John C. Edwards. Principles of NMR. Process NMR Associates LLC, 87A Sand Pit Rd, Danbury CT 06810;. Available from: `http://www.process-nmr.com/pdfs/NMR%20Overview.pdf`.

[6] Tipler PA, Llewellyn RA. Modern Physics, 3rd Edition. W.H. Freeman; 1999.

[7] Hornak JP. The Basics of NMR; 1999. Accessed: 13/07/2012. Available from: `http://www.cis.rit.edu/htbooks/nmr/chap-6/chap-6.htm`.

[8] Suetens P. Fundamentals of medical imaging. 2nd ed. Cambridge University Press; 2009.

[9] Hagmann P, Jonasson L, Maeder P, Thiran JP, Wedeen VJ, Meuli R. Understanding diffusion MR imaging techniques: from scalar diffusion-weighted imaging to diffusion tensor imaging and beyond. Radiographics. 2006;26 Suppl 1:S205–23.

[10] Morley, Gavin W. Still images from animation of a Hahn echo.; 2011. Accessed: 13/07/2012. Available from: `http://upload.wikimedia.org/wikipedia/commons/9/99/SpinEcho_GWM_stills.jpg`.

[11] Oppelt A. Imaging systems for medical diagnostics : fundamentals, technical solutions and applications for systems applying ionization radiation, nuclear magnetic resonance and ultrasound. Publicis Corporate Pub.; 2005.

[12] Masutani Y. MR diffusion tensor imaging: recent advance and new techniques for diffusion tensor visualization. European Journal of Radiology. 2003 Apr;46(1):53–66. Available from: http://dx.doi.org/10.1016/S0720-048X(02)00328-5.

[13] Nucifora PGP, Verma R, Lee SK, Melhem ER. Diffusion-Tensor MR Imaging and Tractography: Exploring Brain Microstructure and Connectivity. Radiology. 2007;245(2):367–384. Available from: http://radiology.rsna.org/content/245/2/367.

[14] Bihan DL, Mangin JF, Poupon C, Clark CA, Pappata S, Molko N, et al. Diffusion Tensor Imaging: Concepts and Applications. Journal of Magnetic Resonance Imaging. 2001;13:534–546.

[15] Bjålie JG, Haug E, Sand O, Sjaastad ØV. Ihminen, fysiologia ja anatomia. 4th ed. WSOY; 2007.

[16] NEUROtiker, Medialansicht eines halbierten menschlichen Gehirns, lateinisch beschriftet.; 2007. Accessed: 17/10/2012. Available from: http://en.wikipedia.org/w/index.php?title=File:Gehirn,_medial_-_beschriftet_lat.svg.

[17] Wakana S, Jiang H, Poetscher NLM, van Zijl PC, Mori S. Fiber tract-based atlas of human white matter anatomy. Radiology. 2004 Jan;230(1):77–87. Available from: http://dx.doi.org/10.1148/radiol.2301021640.

[18] Jones DK, Simmons A, Williams SCR, Horsfield MA. Non-invasive assessment of axonal fiber connectivity in the human brain via diffusion tensor MRI. Magnetic Resonance in Medicine. 1999;42:37–41.

[19] Bode MK, Mattila M, Kiviniemi V, Rahko J, Moilanen I, Ebeling H, et al. White matter in autism spectrum disorders – evidence of impaired fiber formation. Acta Radiol. 2011;52(10):1169–74.

[20] Rutgers DR, Toulgoat F, Cazejust J, Fillard P, Lasjaunias P, Ducreux D. White matter abnormalities in mild traumatic brain injury: a diffusion tensor imaging study. AJNR American journal of neuroradiology. 2008 Mar;29(3):514–9. Available from: http://hal.inria.fr/inria-00502701.

[21] Fitzgerald DB, Crosson BA. Diffusion weighted imaging and neuropsychological correlates in adults with mild traumatic brain injury. Int J Psychophysiol. 2011;Available from: http://www.biomedsearch.com/nih/Diffusion-weighted-imaging-neuropsychological-correlates/21338633.html.

[22] Inglese M, Makani S, Johnson G, Cohen BA, Silver JA, Gonen O, et al. Diffuse axonal injury in mild traumatic brain injury: a diffusion tensor imaging study. J Neurosurg. 2005;103(2):298–303.

[23] Westlye LT, Bjørnebekk A, Grydeland H, Fjell AM, Walhovd KB. Linking an anxiety-related personality trait to brain white matter microstructure: diffusion tensor imaging and harm avoidance. Arch Gen Psychiatry. 2011;68(4):369–77. Available from: http://www.biomedsearch.com/nih/Linking-anxiety-related-personality-trait/21464361.html.

[24] Pierpaoli C, Jezzard P, Basser PJ, Barnett A, Di Chiro G. Diffusion tensor MR imaging of the human brain. Radiology. 1996 Dec;201(3):637–648. Available from: http://radiology.rsna.org/content/201/3/637.abstract.

[25] The Oxford Centre for Functional MRI of the Brain Software Library. Data formats in FSL.; 2012. Accessed: 19/07/2012. Available from: http://www.fmrib.ox.ac.uk/fsl/fsl/formats.html.

[26] Lewis Center for NeuroImaging. MRIConvert: a nifty DICOM converter.; 2012. Accessed: 19/07/2012. Available from: http://lcni.uoregon.edu/~jolinda/MRIConvert/.

[27] Smith SM. Fast robust automated brain extraction. Human Brain Mapping. 2002;17(3):143–155. Available from: http://dx.doi.org/10.1002/hbm.10062.

[28] Nichols TE, Holmes AP. Nonparametric Permutation Tests for Functional Neuroimaging: A Primer with Examples. Human Brain Mapping. 2002;15:1–25.

[29] Smith SM, Nichols TE. Threshold-free cluster enhancement: Addressing problems of smoothing, threshold dependence and localisation in cluster inference. NeuroImage. 2009;44(1):83–98.

[30] VMware, Inc. VMware Player: Run Windows 7, Chrome OS - Free Download for a Virtual PC.; 2012. Accessed: 14/08/2012. Available from: http://www.vmware.com/products/player/.

[31] Andersson JLR, Jenkinson M, Smith S. Non–linear optimisation. FMRIB Technical Report TR07JA1. 2007;p. 16. Available from: http://www.fmrib.ox.ac.uk/analysis/techrep/tr07ja1/tr07ja1.pdf.

[32] Andersson JLR, Jenkinson M, Smith S. Non–linear registration aka Spatial normalisation. FMRIB Technical Report TR07JA2. 2007;p. 21. Available from: http://www.fmrib.ox.ac.uk/analysis/techrep/tr07ja2/tr07ja2.pdf.

[33] Rueckert D, Sonoda LI, Hayes C, Hill DLG, Leach MO, Hawkes DJ. Nonrigid registration using free-form deformations: Application to breast MR images. IEEE Transactions on Medical Imaging. 1999;18:712–721.

[34] FSL Evaluation and Example Data Suite, Timings Table.; 2012. Accessed: 17/11/2012. Available from: http://fsl.fmrib.ox.ac.uk/fsl/feeds/doc/timings.html.

[35] Bullmore ET, Suckling J, Overmeyer S, Robe-Hesketh S, Taylor E, Brammer MJ. Global, Voxel and Cluster Tests, by Theory and Permutation, for a Difference Between Two Groups of Structural MR Images of the Brain. IEEE Trans Med Imaging. 1999;p. 32–42.

[36] Jones DK, Cercignani M. Twenty-five pitfalls in the analysis of diffusion MRI data. NMR in Biomedicine. 2010;23(7):803–820. Available from: http://dx.doi.org/10.1002/nbm.1543.

[37] Goldberg MP, Ransom BR. New light on white matter. Stroke. 2003;34(2):330–2. Available from: http://www.biomedsearch.com/nih/New-light-white-matter/12574526.html.

[38] Richards T, Stevenson J, Crouch J, Johnson LC, Maravilla K, Stock P, et al. Tract-based spatial statistics of diffusion tensor imaging in adults with dyslexia. AJNR Am J Neuroradiol. 2008;29(6):1134–9. Available from: http://www.biomedsearch.com/nih/Tract-based-spatial-statistics-diffusion/18467520.html.

[39] Emmer BJ, Veer IM, Steup-Beekman GM, Huizinga TWJ, van der Grond J, van Buchem MA. Tract-based spatial statistics on diffusion tensor imaging in systemic lupus erythematosus reveals localized involvement of white matter tracts. Arthritis Rheum. 2010;62(12):3716–21. Available from: http://www.biomedsearch.com/nih/Tract-based-spatial-statistics-diffusion/20722009.html.

[40] Barnea-Goraly N, Chang KD, Karchemskiy A, Howe ME, Reiss AL. Limbic and corpus callosum aberrations in adolescents with bipolar disorder: a tract-based spatial statistics analysis. Biol Psychiatry. 2009;66(3):238–44. Available from: http://www.biomedsearch.com/nih/Limbic-corpus-callosum-aberrations-in/19389661.html.

Appendices

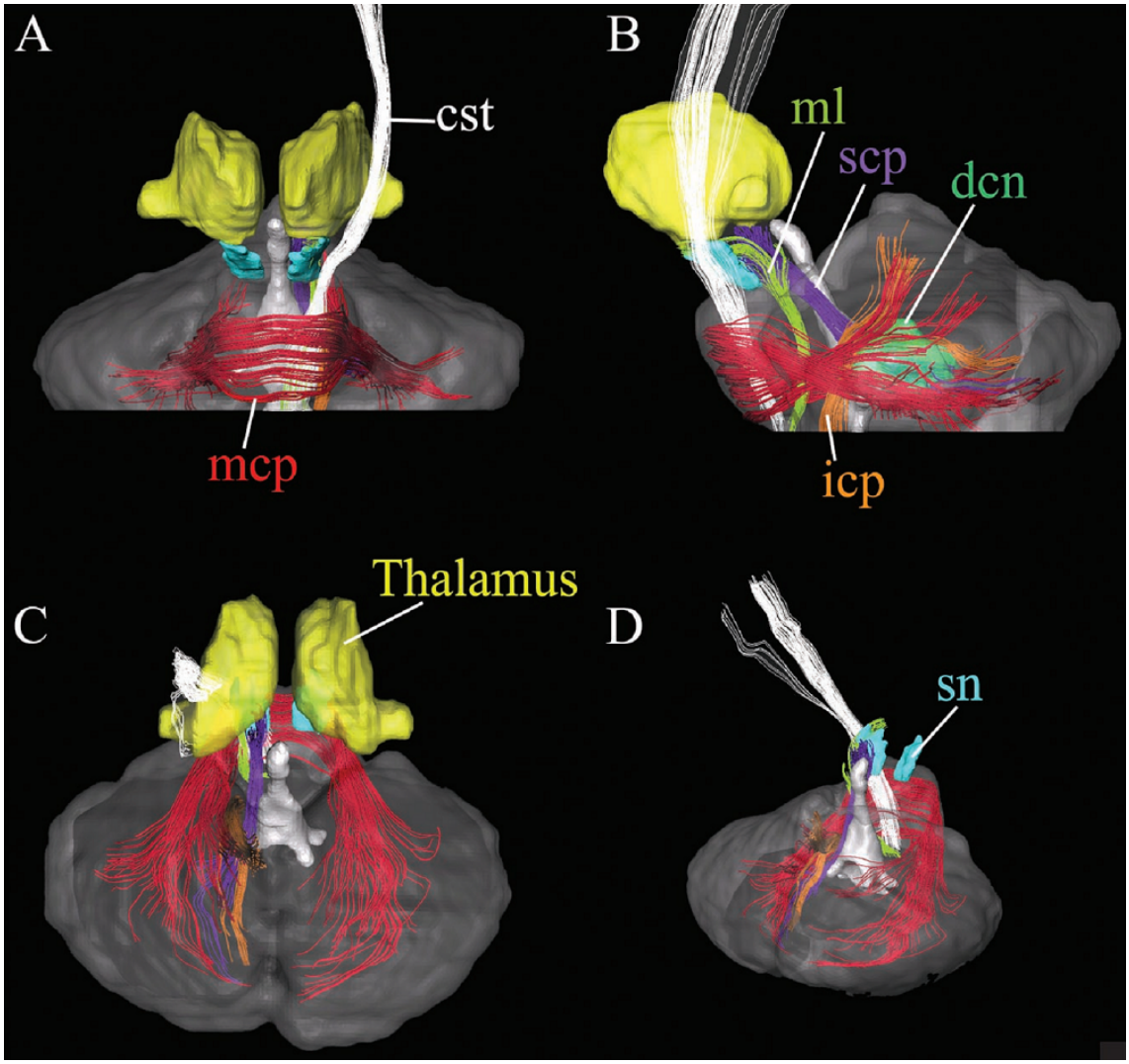

Appendix 1: 3D reconstruction of brainstem tracts from four different angles; A) anterior view, B) left lateral view, C) superior view, D) oblique view from right posterior angle. Tract abbreviations: cst (white), corticospinal tract; scp (purple), superior cerebellar peduncle; mcp (red), middle cerebellar peduncle; icp (orange), inferior cerebellar peduncle; and ml (light green), medial lemniscus. For clarification subtantia nigra (sn, blue), deep cerebellar nuclei (dcn, dark green) and thalamus (yellow) are shown. [17]

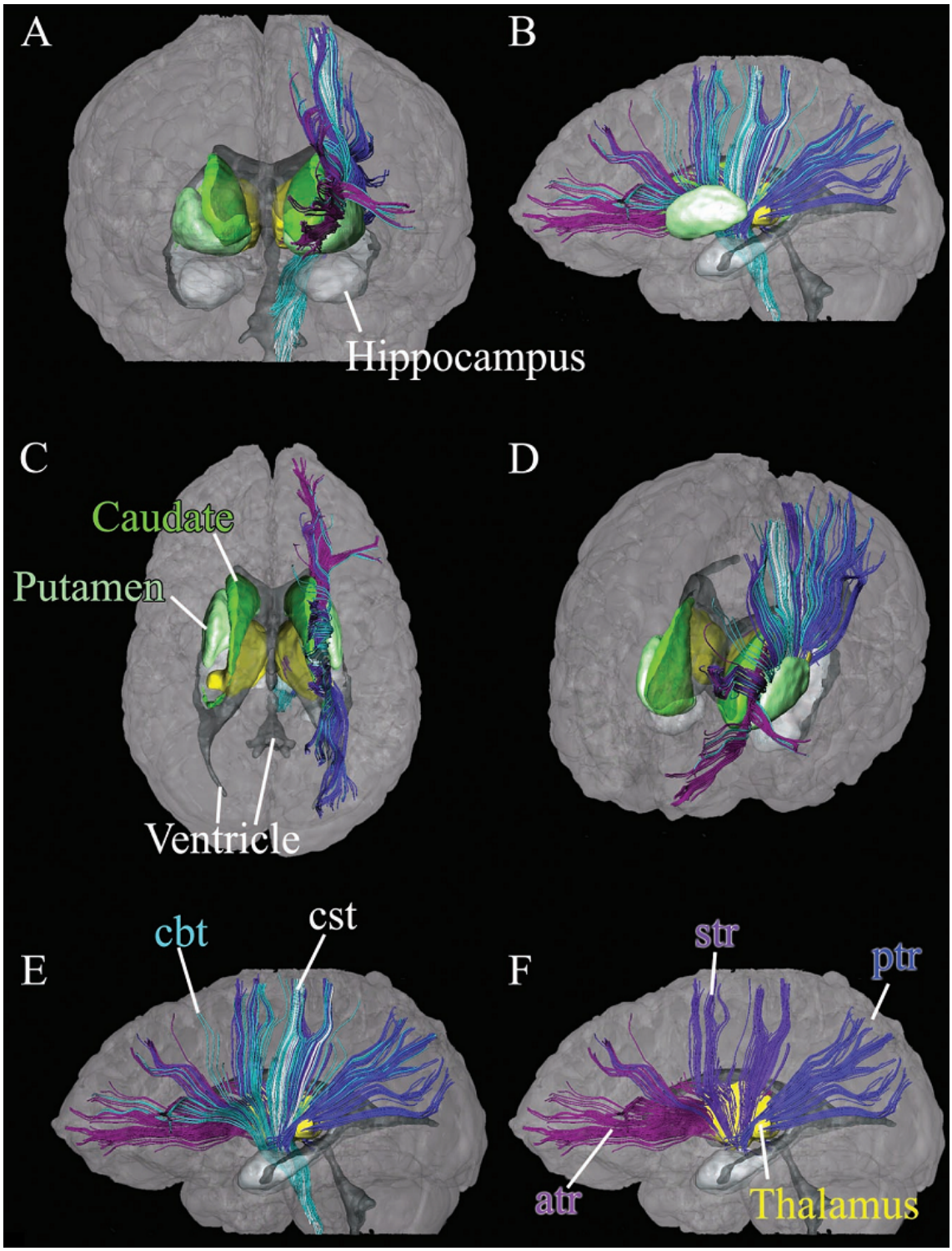

Appendix 2: Projection and thalamic fibers; A) anterior view, B) left lateral view, C) superior view, D) oblique view from right anterior angle. Fiber abbreviations: cbt (light blue), corticobulbar tracts; cst (white), corticospinal tract; atr (bright blue), anterior thalamic radiation; str (purple), superior thalamic radiation; and ptr (dark blue), posterior thalamic radiation. For clarification additional lateral views, E and F, are presented. [17]

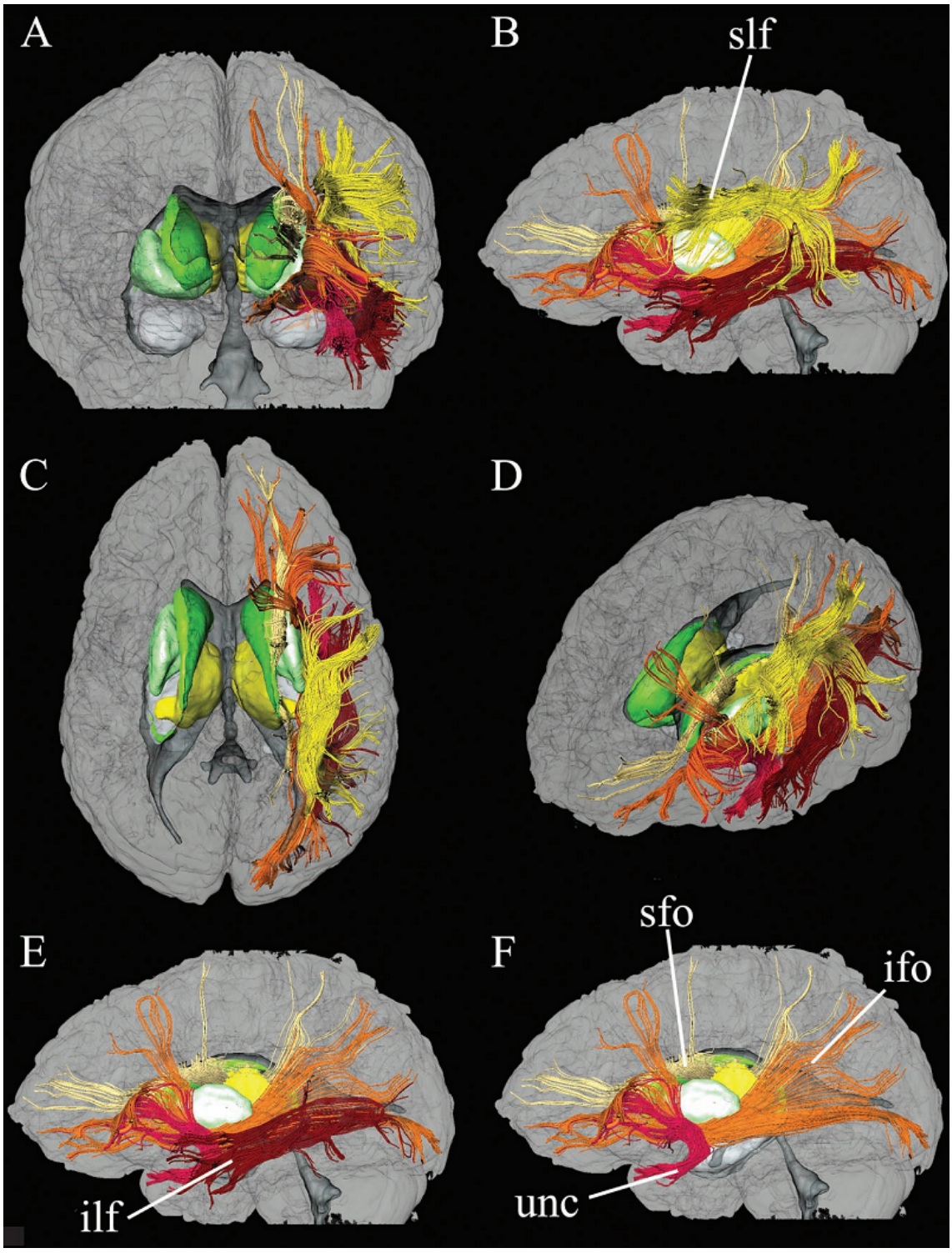

Appendix 3: Association fibers; A) anterior view, B) left lateral view, C) superior view, D) oblique view from right anterior angle. Fiber abbreviations: slf (yellow), superior longitudinal fasciculus; ilf (brown), inferior longitudinal fasciculus; sfo (beige), superior fronto-occipital fasciculus; ifo (orange), inferior fronto-occipital fasciculus; and unc (red), uncinate fasciculus. For clarification additional lateral views without superior longitudinal fasciculus (E and F) are presented. [17].

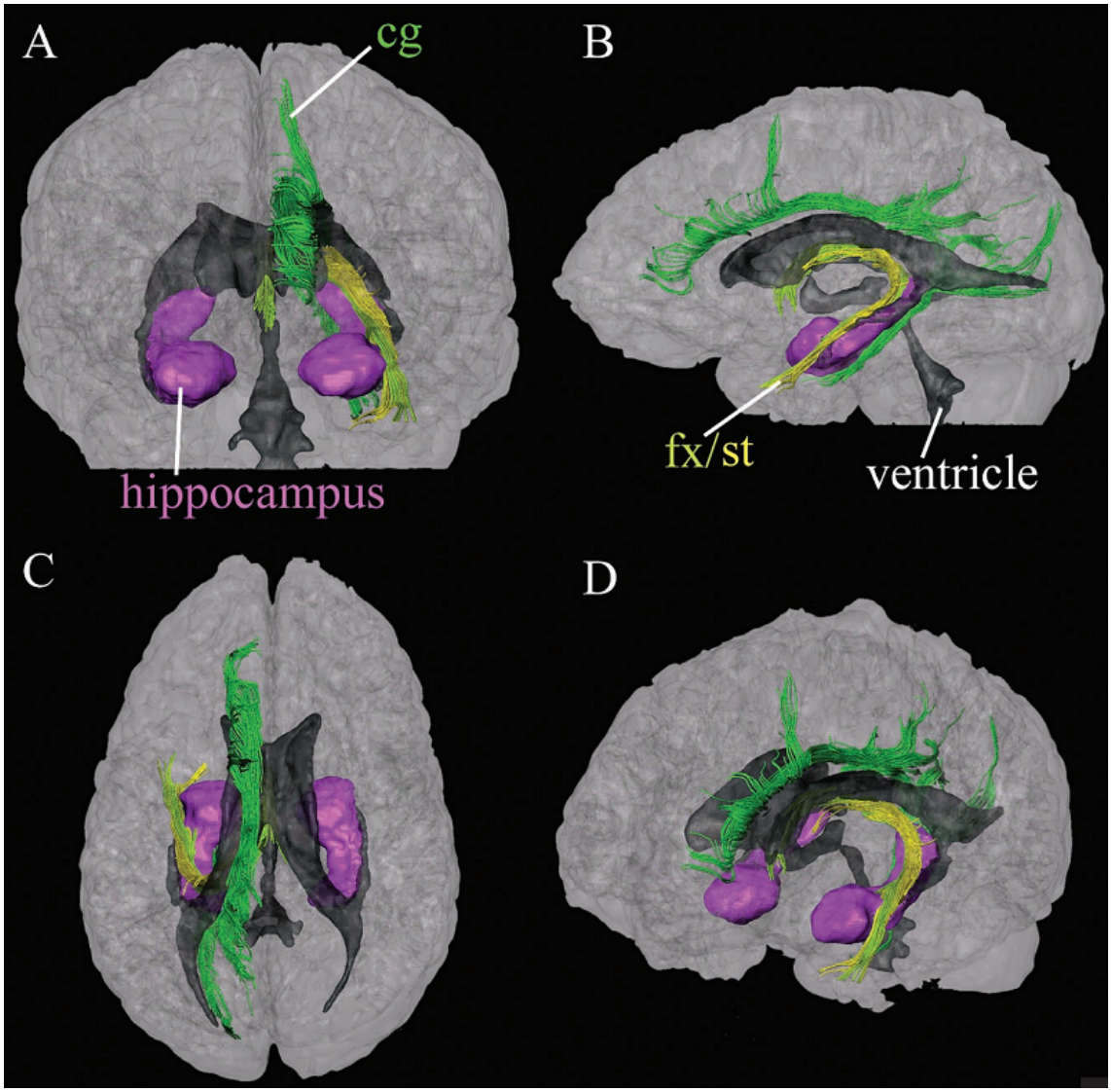

Appendix 4: Limbic system tracts; A) anterior view, B) left lateral view, C) superior view, D) oblique view from right anterior angle. Reconstructed fiber abbreviations: cg (dark green), cingulum; fx (light green), fornix; and st (yellow), stria terminalis. For clarification hippocampus and amygdala (purple) are shown. [17]

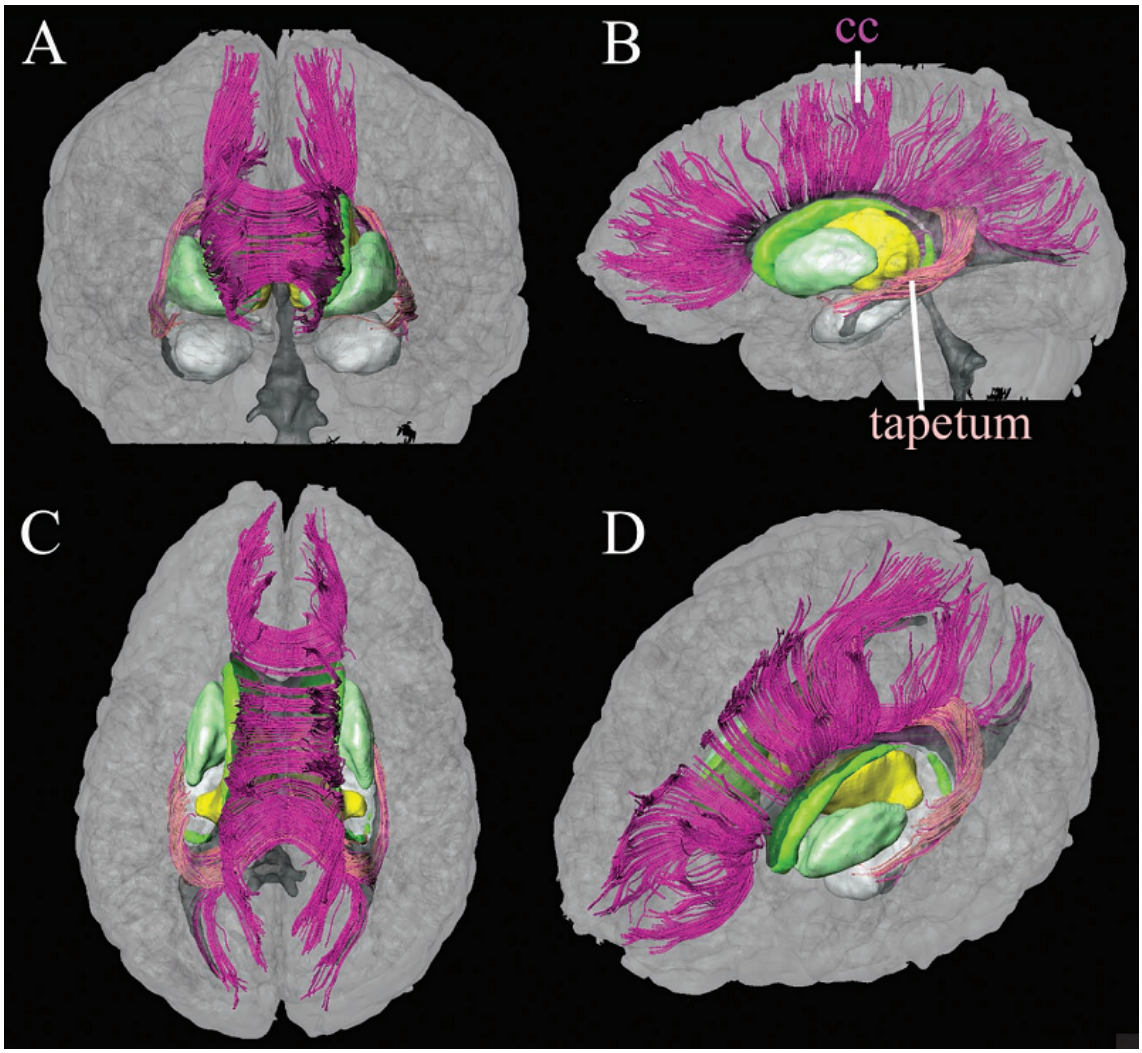

Appendix 5: Callosal fibers; A) anterior view, B) left lateral view, C) superior view, D) oblique view from right anterior angle. Corticocortical tract connections (cc, magenta) through the corpus callosum and tracts projecting to temporal lobe (tapetum, pink) are visible. [17]

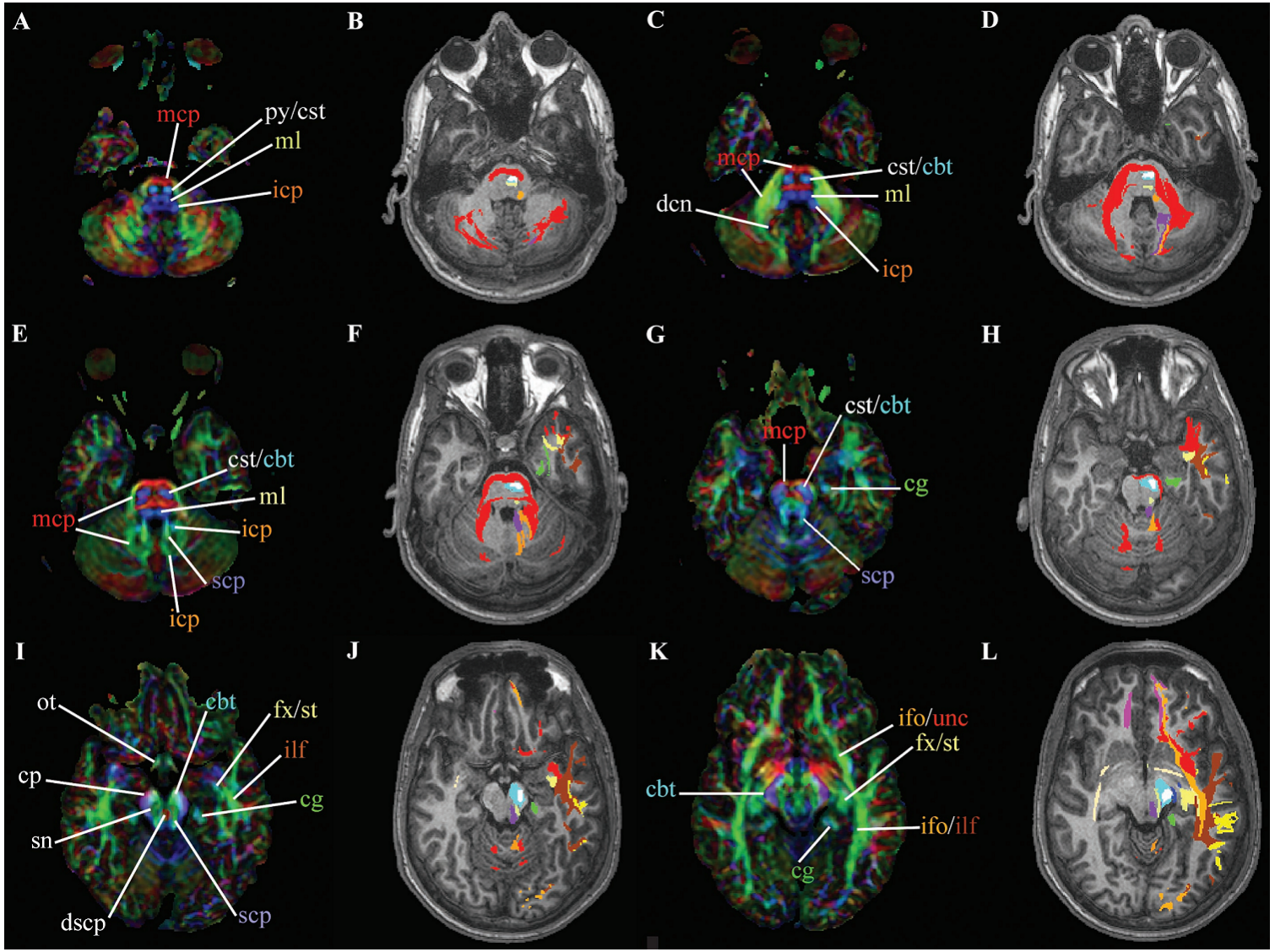

Appendix 6: Transverse fiber structure (1/2) presented in diffusion colormaps and white matter parcellation maps. Color coded diffusion maps include assigned locations of various fiber tracts. Parcellation map fiber trajectories are colored with same colors as used in appendices 2-6. Abbreviations used in appendix 7 and 8: ac= anterior commissure, acr= anterior region of corona radiata, alic= anterior limb of internal capsule, cbt= corticobulbar tract, cg= cingulum, cp= cerebral peduncle, cst= corticospinal tract, dscp= decussation of superior cerebellar peduncle (scp). (*Continued in appendix 8.*) [17]

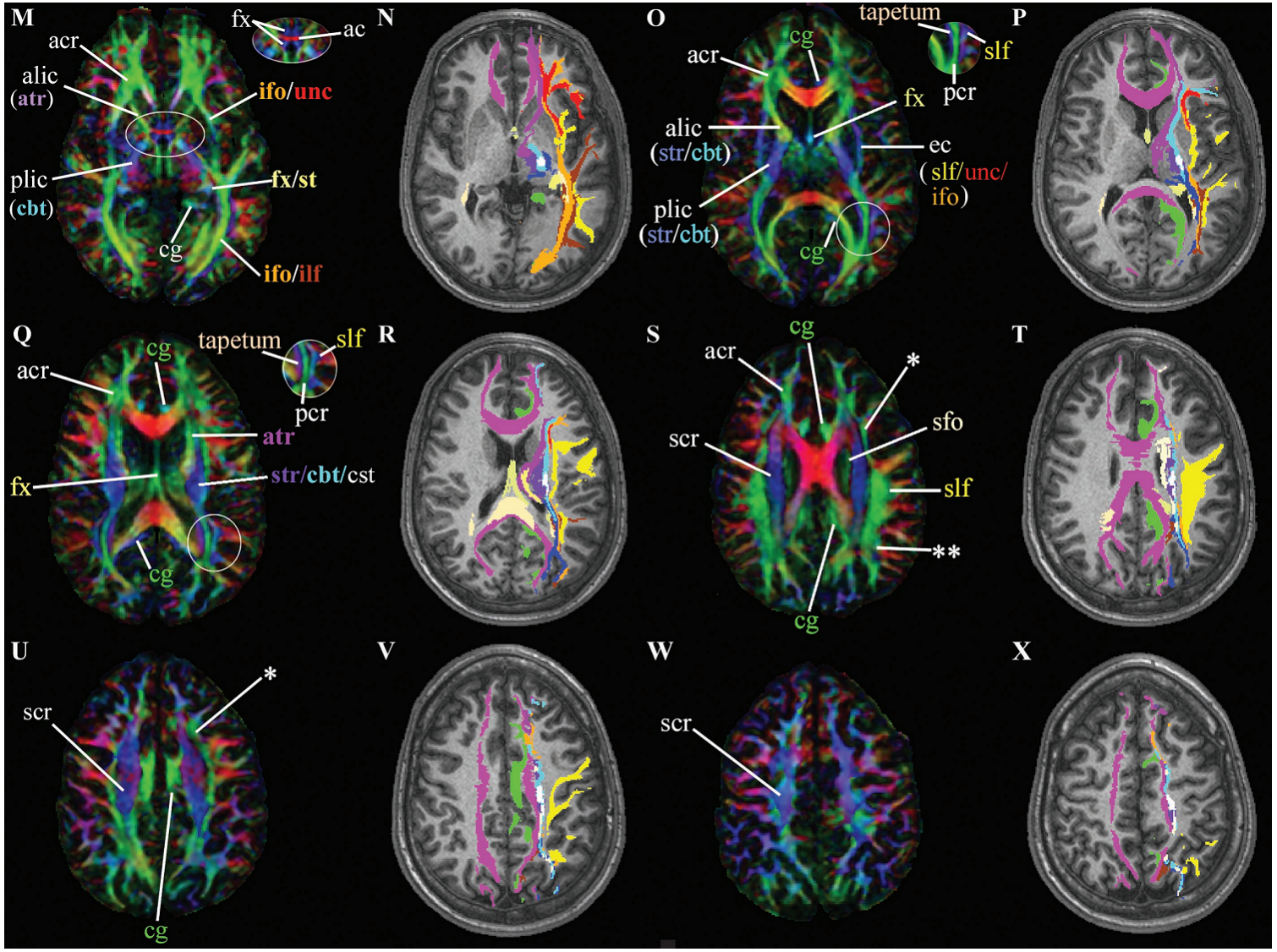

Appendix 7: Transverse fiber structure (2/2). fx= fornix, icp= inferior cerebellar peduncle, ifo= inferior fronto-occipital fasciculus, ilf= inferior longitudinal fasciculus, mcp= middle cerebellar peduncle, ml= medial lemniscus, ot= optic tract, pcr= posterior region of corona radiata, plic= posterior limb of internal capsule, py= pyramidal tract, scr= superior region of internal capsule, sfo= superior fronto-occipital fasciculus, slf= superior longitudinal fasciculus, sn= substantia nigra, st= stria terminalis, unc= uncinate fasciculus,*= short-range associationfibers, **= vertical occipital fasciculus. [17]

Appendix 8: Optional arguments available for the Randomise program, version 2.9.

Parameter	**Description**
-D	Demean data temporally before model fitting.
-1	Perform 1-sample group-mean test instead of generic permutation test.
-m <mask>	Brain mask image input.
-f <fts>	F contrasts file.
-e <grp>	Exchangeability block labels file.
--effective_design <d.mat>	Alternative design for determining valid permutations.
-q	Print out how many unique permutations would be generated and exit.
-Q	Print out information required for parallel mode and exit.
-n <n_perm>	Number of permutations (default 5000, set 0 for exhaustive).
-x	Output voxelwise p-value images.
--fonly	Calculate f-statistics only.
-T	Carry out Threshold-Free Cluster Enhancement.
--T2	Same as above, but with 2D optimisation (e.g. for TBSS data); H=2, E=1, C=26.
-c <thresh>	Cluster based thesholding.
-C <thresh>	Cluster-mass based thresholding.
-F <thresh>	F cluster thresholding.
-S <thresh>	F cluster-mass thresholding.
-v <std>	Use variance smoothing (std in mm).
-h, --help	Display help message.
--quiet	Switch off diagnostic messages.
--twopass	Cluster normalisation thresholding.
-R	Output raw (unpermuted) statistic images.
-P	Output permutation vector text file.
-N	Output null distribution text files.
--norcmask	Do not remove constant voxels from mask.
--seed <seed>	Specific integer seed for random number generator.
--tfce_H <H>	TFCE height parameter (default=2).
--tfce_E <E>	TFCE extent parameter (default=0.5).
--tfce_C <C>	TFCE connectivity (6 or 26, default=6).

Appendix 9: Additional options available for *cluster* subprogram.

Parameter	**Description**
-o	Filename for output cluster index.
--othresh	Filename for output of thresholded image.
--olmax	Filename for output of local maxima text file.
--olmaxim	Filename for output of local maxima volume.
--osize	Filename for output of size image.
--omax	Filename for output of max image.
--omean	Filename for output of mean image.
--opvals	Filename for image output of log p-values.
-p	p-threshold for clusters.
--peakdist	Minimum distance between local maxima/minima, in mm (default 0).
-c	Filename of input cope volume.
--volume	Number of voxels in the mask.
-d	Smoothness estimate = sqrt(det(Lambda)).
--fractional	Interprets the threshold as a fraction of the robust range.
--connectivity	The connectivity of voxels (default 26).
--mm	use millimeters instead of voxels as coordinates.
--min	Find minima instead of maxima.
--no_table	Suppresses printing of the table info.
--minclustersize	Prints out minimum significant cluster size.
-x	Filename for Linear: input -> standard-space transform. Non-linear: input -> highres transform.
--stdvol	Filename for standard-space volume.
-n	Number of local maxima to report.
-v	Switch on diagnostic messages.
-h	Display help message.
--warpvol	Filename for warpfield.

Appendix 10: MRI analysis and processing tools available in FSL.

Structural MRI

Tool	Description
BET	Brain Extraction Tool. Segments brain tissue data and deletes non brain data. Can also estimate inner and outer skull surfaces from good quality T1 and T2 input images.
FAST	FMRIB's Automated Segmentation Tool for brain tissue types.
FLIRT	FMRIB's Linear Image Registration Tool. Robust and accurate automated tool for linear brain image registration.
FNIRT	FMRIB's Non-linear Image Registration Tool. A versatile tool for nonlinear brain image registrations.
FIRST	FMRIB's Integrated Registration and Segmentation Tool for subcortical model based brain segmentation. Uses a provided set of manually segmented images as models.
FUGUE	FMRIB's Utility for Geometrically Unwarping EPIs. Unwarps geometric distortion in echo planar images using B_0 field maps.
SIENA	Structural Image Evaluation, using Normalisation, of Atrophy; structural brain change analysis, for estimating brain atrophy.
FSL-VBM	Voxelwise analysis of multi-subject structural MRI data. VBM-style analysis using FSL tools, for voxelwise analysis of grey-matter density.
SUSAN	Nonlinear Noise Reduction.

Functional MRI

Tool	Description
FEAT	FMRI Expert Analysis Tool. Simple but efficient analysis tool for FMRI time series data.
MELODIC	Multivariate Exploratory Linear Optimized Decomposition into Independent Components. Decomposes data sets into different spatial and temporal components and analyzes them.
FLOBS	FMRIB's Linear Optimal Basis Sets. Generates optimal basis sets for use in haemodynamic response function convolution in FMRI linear modelling.
FABBER	Fast ASL & BOLD Bayesian Estimation Routine. Nonlinear modeling and estimation of blood oxygen level dependent and cerebral blood flow values from dual echo arterial spin labeling images.

Diffusion MRI

Tool	Description
FDT	FMRIB's Diffusion Toolbox. A versatile toolbox for diffusion weighted image processing and analysis.
TBSS	Tract-Based Spatial Statistics; a voxelwise analysis program for multi-subject diffusion data. A part of FMRIB's Diffusion Toolbox.

Appendix 11: Other tools available in FSL.

Tool	**Description**
POSSUM	Physics-Oriented Simulated Scanner for Understanding MRI. A MRI simulator which generates MRI and FMRI images from input 4D volumes. Mostly an educational tool.
Inference	Various tools for inference and thresholding. Includes Radomise tool used in the TBSS tool.
FSLView	An interactive display tool for viewing 3D and 4D ANALYZE and NIfTI files.
Atlases	Various complementary brain atlases created from multiple human subjects. Atlases are integrated into FSLView.
FSLUTILS	Miscellaneous command line utilities for converting and processing ANALYZE and NIfTI images.
MISCVIS	Miscellaneous visualization related utilities for image overlays and 3D or 4D image conversion to 2D image slices.